iScience

Article

The *Iroquois* (*Iro/Irx*) homeobox genes are conserved Hox targets involved in motor neuron development

Graphical abstract

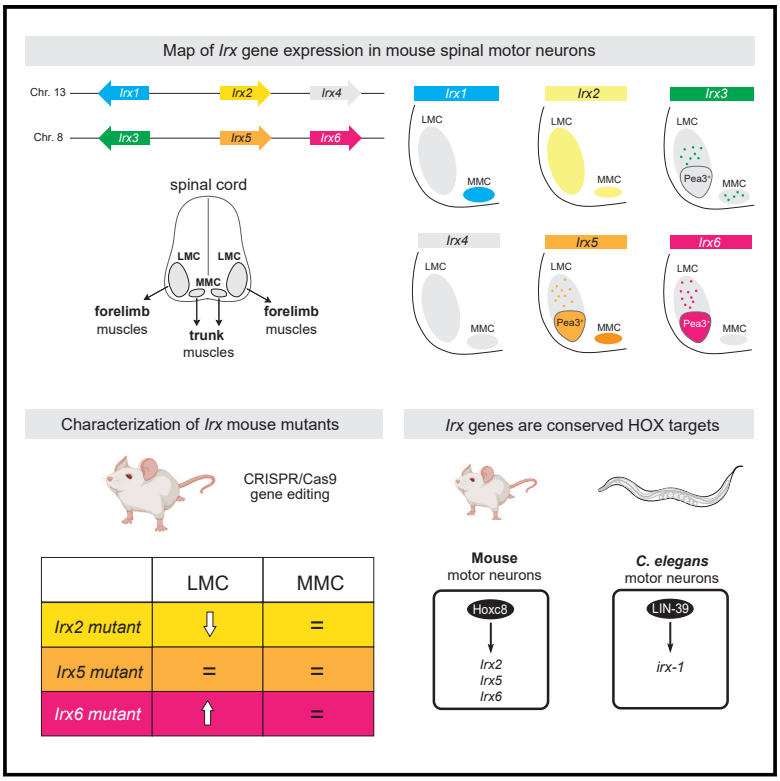

Highlights

- A detailed map of *Irx* gene expression in mouse spinal motor neurons
- *Irx2* is required for the development of limb-innervating motor neurons
- *Irx6* limits the number of limb-innervating motor neurons in brachial domains
- Hox proteins control *Irx* gene expression in *C. elegans* and mouse motor neurons

Authors

Catarina Catela, Stavroula Assimacopoulos, Yihan Chen, Konstantinos Tsioras, Weidong Feng, Paschalis Kratsios

Correspondence

pkratsios@uchicago.edu

In brief

Molecular biology; Neuroscience

Catela et al., 2025, iScience *28*, 112210
April 18, 2025
https://doi.org/10.1016/j.isci.2025.112210

CellPress

iScience

CellPress
OPEN ACCESS

Article

The *Iroquois* (*Iro*/*Irx*) homeobox genes are conserved Hox targets involved in motor neuron development

Catarina Catela,[1,2] Stavroula Assimacopoulos,[1,2] Yihan Chen,[1,2] Konstantinos Tsioras,[1,2] Weidong Feng,[1,2] and Paschalis Kratsios[1,2,3,*]

[1]Department of Neurobiology, University of Chicago, Chicago, IL 60637, USA
[2]Neuroscience Institute, University of Chicago, Chicago, IL 60637, USA
[3]Lead contact
*Correspondence: pkratsios@uchicago.edu
https://doi.org/10.1016/j.isci.2025.112210

SUMMARY

The *Iroquois (Iro/Irx)* homeobox genes encode transcription factors with fundamental roles in animal development. Despite their link to various congenital conditions in humans, our understanding of *Iro/Irx* gene expression, function, and regulation remains incomplete. Here, we conducted a systematic expression analysis of all six mouse *Irx* genes in the embryonic spinal cord. We found that *Irx1*, *Irx2*, *Irx3*, *Irx5*, and *Irx6* are expressed in specific groups of motor neurons (MNs). Further, we employed CRISPR-Cas9 gene editing to uncover essential but distinct roles for *Irx2* and *Irx6* in MN development. We also found that HOX proteins, which are conserved regulators of MN development across species, control *Irx* gene expression both in mouse and *Caenorhabditis elegans* MNs. Altogether, our study provides insights into *Iro/Irx* expression and function in the developing spinal cord and uncovers an ancient gene regulatory relationship between HOX and *Iro/Irx* genes.

INTRODUCTION

The *Iroquois homeobox (Irx)* genes encode a family of conserved homeodomain transcription factors.[1] They play crucial roles in the regulation of various developmental processes, particularly in cell specification and differentiation during embryonic development.[2] First discovered in the fruit fly *Drosophila melanogaster*, the *Irx* genes were named after their distinct mutant phenotype; *Iroquois* mutant flies display a wide band of sensory organs across the central region of mesothorax – a pattern resembling the hairstyle worn by members of the Iroquois Confederacy.[3] Except for the nematode *Caenorhabditis elegans*, which has a single ancestral *Iroquois* gene *(irx-1)*, *Irx* genes are typically organized in genomic clusters. Three genes (*ara*, *caup*, and *mirr*) are present in a single cluster in *Drosophila*, whereas six genes in mice (*Irx1-6*) and humans (*IRX1-6*) are found in two separate chromosomal clusters (Figures 1A and 1B). Irx proteins bind DNA through a highly conserved 63 amino acid-long homeodomain of the TALE (three-amino acid loop extension) class and carry a distinct 13 amino acid domain (Iro box) involved in protein-protein interactions (Figure 1C).[4]

Emerging evidence shows that *Irx* gene expression spans large territories in early embryos but becomes restricted to distinct cell types and tissues at later stages of development.[1,2] As such, *Irx* genes not only control embryonic patterning and cell specification, but also play later roles in tissue differentiation and function. In *Drosophila*, *Irx* genes specify large territories in the developing eye and wing disc.[1,6,7] In vertebrates, they control cell specification and function in the developing heart,[8] lung,[9] kidney,[10,11] pancreas,[12] gonad,[13] and limb.[14] Mutations in human *IRX* genes can lead to a range of phenotypic effects, such as heart defects, craniofacial abnormalities, and cancer.[8,15–17] Much of our current knowledge on *Irx* genes, however, derives from studies in the murine heart, where a systematic expression pattern analysis of all six *Irx* genes has been complemented with individual and compound *Irx* mutant analyses.[8,18,19] These studies revealed both essential and redundant functions for *Irx* genes, and further demonstrated that Irx proteins can either act as activators or repressors of gene expression. Beyond the developing heart, systematic expression and mutant analyses for *Irx* genes are currently lacking in other vertebrate tissues (e.g., kidney, brain, and spinal cord), limiting our understanding of how these highly conserved transcription factors control animal development.

In the nervous system, *Iro/Irx* genes play crucial roles during early and late stages of development.[2] For example, growing evidence suggests their requirement for the initial specification of vertebrate neuroectoderm, the first step of nervous system development. In *Xenopus*, *Iro* genes specify the neural territory during gastrulation.[20–22] Both in *Drosophila* and vertebrates, *Iro/Irx* genes are known to regulate proneural genes essential for the development of neuroectodermal progenitor cells.[20,23,24] Subsequently, *Iro/Irx* genes subdivide the developing neuroectoderm and promote regional identities along the dorsoventral

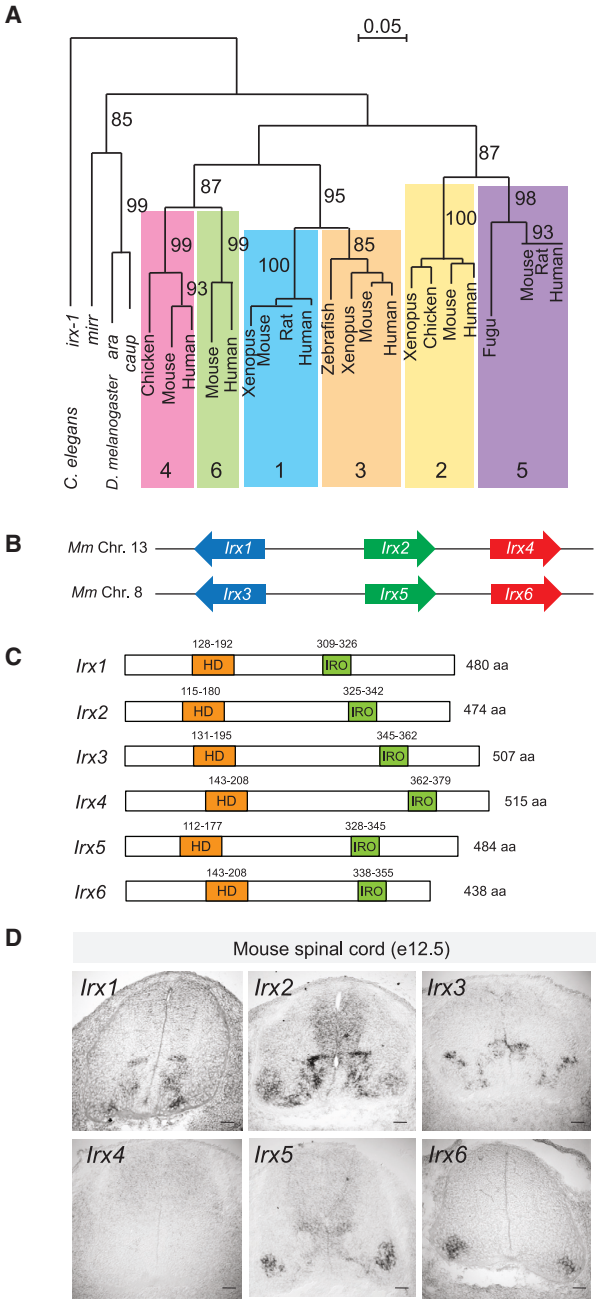

Figure 1. Expression pattern of all six *Irx* genes in mouse spinal motor neurons

(A) Phylogenetic tree of the *Iro/Irx* gene family. Adapted from.[5] Scale bar: percentage of sequence divergence. Numbers above branches: percentage of times the branch was found in 200 bootstrap replicates. Brackets highlight the clustering of vertebrate genes into six orthologous groups.

(B) Schematic of the two *Irx* chromosomal clusters in mice.

(C) Schematic of the mouse Irx protein domains. Each protein has a highly conserved 63 amino acid-long homeodomain and a distinct 16 amino acid-long Iro box domain.

(D) RNA ISH analysis of *Irx1*, *Irx2*, *Irx3*, *Irx4*, *Irx5*, and *Irx6* on cross-sections of e12.5 wild-type mouse spinal cords. Brachial (C4-T1) domain. $N = 4$. Scale bar: 50 μm. See also Figure S3.

(D-V) axis of the developing spinal cord and anterior-posterior axis of the brain.[2,25–27] They do so by generating sharp boundaries between dividing progenitor cells through mutual cross-repression with other transcription factors. In progenitor cells, Irx3 cross-represses Olig2 in the spinal cord, Six3 in the forebrain, and Hnf1 in the hindbrain.[28–31]

During later stages of neural development, *Iro/Irx* genes are best characterized in the developing retina, where *Drosophila* and mouse studies revealed essential roles in neurogenesis[32,33] and cell specification.[1,7,34,35] In the mouse retina, *Irx4* controls axon guidance, whereas *Irx5* and *Irx6* are necessary for interneuron terminal differentiation.[36–38] Moreover, *Irx* genes have been implicated in cerebellum formation,[39] serotonergic neuron differentiation,[40] and postnatal neurogenesis in the hypothalamus.[41] Human *IRX3* and *IRX5* have been associated with obesity, and mouse studies demonstrated that hypothalamic *Irx3* and *Irx5* are involved in feeding behavior and metabolism.[42–45] Further, *IRX5* mutations cause a recessive congenital disorder affecting brain, face, blood, and heart development.[15] Altogether, multiple studies to date have reported essential roles for *Irx* genes in various parts (retina, cerebellum, and hypothalamus) of the developing central nervous system (CNS), except the spinal cord, where our knowledge of *Irx* gene function remains rudimentary.

How is *Iro/Irx* gene expression controlled during development? During early patterning, studies in *Drosophila* showed that *Iro* genes are activated by multiple signaling pathways, such as Hedgehog, Wingless, JAK/STAT, and EGFR.[46,47] In the vertebrate neural plate, *Irx/Iro* gene expression is activated by Wnt and repressed by BMP signaling.[22,48] During later stages of CNS development, *Irx2* is a target of the FGF8/MAP kinase cascade in the midbrain and *Irx3* is repressed by Shh signaling in the spinal cord.[39,49] However, how *Irx/Iro* gene expression is regulated in the context of post-mitotic neurons remains largely unknown.

Here, we report a detailed expression map of all six mouse *Irx* genes in the embryonic spinal cord, revealing unique and overlapping expression patterns in distinct populations of post-mitotic neurons. Through CRISPR/Cas9 gene editing, we engineered mouse mutants for *Irx2, Irx5,* and *Irx6* and uncover essential (*Irx2*, *Irx6)* and dispensable *(Irx5)* roles in spinal MN development. Lastly, we provide evidence – both in *C. elegans* and mice – that Hox transcription factors activate *Irx* gene expression in post-mitotic MNs, exposing an ancient gene regulatory relationship between two highly conserved families of clustered transcription factors.

RESULTS

A detailed map of *irx* gene expression in mouse spinal motor neurons

In mice, *Irx* genes are expressed in various domains of the developing nervous system,[50–54] but their expression in post-mitotic neurons is poorly defined. Here, we systematically investigated the expression of all six mouse *Irx* genes in the developing spinal cord at the brachial (also referred to as "cervical") domain (C4-T1) (Figure 2A). We focused on embryonic day 12.5 (e12.5), as most post-mitotic spinal neurons have been generated by that stage. RNA *in situ* hybridization (ISH) showed that *Irx1, Irx2,*

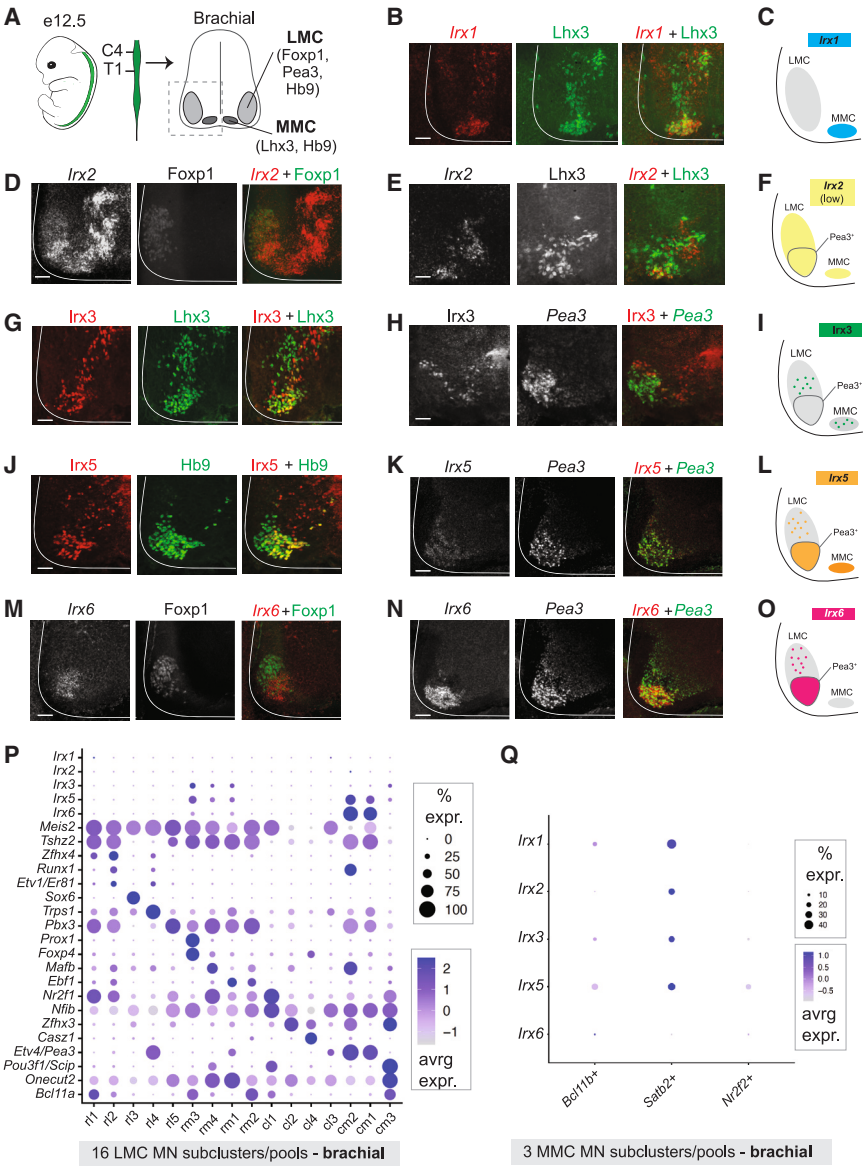

Figure 2. Expression of *Irx1, Irx2, Irx3, Irx5,* and *Irx6* in specific motor columns

(A) Brachial spinal domain (C4-T1) in an e12.5 mouse. Cross-section: LMC and MMC neurons at the ventral region of the spinal cord.

(B) *Irx1* FISH coupled with Lhx3 antibody staining shows *Irx1* expression (red) is detected in Lhx3-expressing MNs (green) of the MMC.

(C) Schematic of *Irx1* expression.

(D and E) *Irx2* FISH combined with immunostaining for Foxp1 (D) or Lhx3 (E) reveals *Irx2* expression (red, also converted to white for better contrast) is detected in LMC (D) and MMC (E) neurons.

(F) Schematic of *Irx2* expression.

(G) Double immunostaining for Irx3 and Lhx3 shows Irx3 (red) is expressed in a small population of Lhx3-positive MNs (green).

(H) Irx3 antibody staining combined with *Pea3* RNA FISH reveals almost no co-localization of Irx3 protein (red) to *Pea3*-expressing MNs (green) of the ventral LMC but expression in a small population of dorsal LMC MNs.

(I) Schematic of *Irx3* expression.

(J) Double immunofluorescence reveals Irx5 expression (red) in Hb9-positive cells (green).

(K) Two-color RNA FISH shows *Irx5* expression (red) is detected in *Pea3*-expressing MNs of the ventral LMC.

(L) Schematic of *Irx5* expression.

(M) *Irx6* RNA (red) colocalizes with Foxp1 protein (green) in the ventral LMC.

(N) Two-color RNA FISH reveals *Irx6* expression (red) in *Pea3*-expressing MNs.

(O) Schematic of *Irx6* expression. B-O: e12.5 spinal cord, $N = 4$. (P-Q) Dot plots show *Irx1*, *Irx2*, *Irx3*, *Irx5*, and *Irx6* transcripts in MN subclusters/pools previously identified in the e13.5 mouse brachial spinal cord. scRNA-Seq data analyzed from.[56]

(P) LMC subclusters/pools are defined by the combinatorial expression of various TFs. Known MN pool markers include: *Etv1/Er81, Etv4/Pea3, Pou3f1/Scip*.

(Q) Three MMC subclusters/pools previously defined by *Bcl11b, Satb2*, or *Nr2f* expression. rm: rostral medial; rl: rostral lateral; cl: caudal lateral; cm: caudal medial. Size of dots indicates the percentage of cells expressing each *Irx* gene. Color code indicates average expression levels. Scale bar: 50 μm. See also Figures S1 and S2.

Irx3 and *Irx5* are mostly confined to medial and ventral regions of the spinal cord, whereas *Irx6* expression is specific to the ventro-lateral region where it overlaps with *Irx5* (Figure 1D). Consistent with a previous report at stages earlier than e12.5,[50] we did not detect expression of *Irx4* (Figure 1D), the most divergent member of the vertebrate *Irx* gene family.[55]

As the majority of *Irx* expression occurs in the ventral region of the spinal cord, which is known to contain post-mitotic motor neurons (MNs), we focused our analysis on these cells. At the brachial domain (C4-T1) of the spinal cord, MNs are mainly organized into two columns. The lateral motor column [LMC] contains forelimb-innervating MNs necessary for reaching, grasping, and locomotion, whereas the medial motor column [MMC] contains axial muscle (trunk)-innervating MNs required for postural control (Figure 2A).[57] At e12.5, post-mitotic MNs (LMC or MMC) can be unambiguously distinguished by using established molecular markers for motor columns (LMC: Foxp1; MMC: Lhx3; LMC and MMC: Hb9; a subpopulation of LMC: Pea3)[58–60] (Figure 2A). To generate a detailed map of *Irx* expression in post-mitotic MNs of the e12.5 brachial spinal cord, we evaluated expression of five mouse *Irx* genes (*Irx1, Irx2, Irx3, Irx5, Irx6*) with RNA fluorescent ISH (FISH).

By coupling RNA FISH for *Irx1* with immunofluorescence for the MMC marker Lhx3, we found that *Irx1* is expressed in MMC neurons (Figures 2B and 2C). Through similar double labeling strategies that rely on RNA FISH and/or immunofluorescence, we determined that: (a) *Irx2* is expressed in MMC and LMC neurons (including the Pea3 pool of MNs) (Figures 2D–2F

and S1A), (b) *Irx3* mRNA and protein are present in MMC neurons and in a small population of LMC neurons (located dorsally to the Pea3 MN pool) (Figures 2G–2I and S1B), (c) *Irx5* mRNA and protein are detected in MMC neurons and the Pea3 pool (Figures 2J–2L and S1C), and (d) *Irx6* mRNA is primarily expressed in the Pea3 pool within the LMC neurons (Figures 2M–2O). In addition to MNs, *Irx1, Irx2, Irx3*, and *Irx5* are expressed in other spinal cell types close to the midline, likely progenitor cells and various types of interneurons (Figure 2).

At the protein level, we evaluated nine commercially available Irx antibodies by performing immunofluorescence staining in the mouse spinal cord (Table S1). We found two antibodies that display specificity; one against Irx3 and another against Irx5 (Table S1). Antibody staining against Irx3 and Irx5 yielded expression patterns similar to the ones observed with *Irx3* and *Irx5* RNA ISH (Figures 1J, 2G, and 2J).

To increase the cellular resolution of *Irx* gene expression, we analyzed recently published single-cell RNA sequencing (scRNA-seq) data of e13.5 MNs from the mouse spinal cord at the brachial domain.[56] The scRNA-seq study revealed 16 subclusters of LMC and three subclusters of MMC MNs, with each subcluster likely representing one or more MN pools.[56] In Figures 2P and 2Q, we report the expression patterns of *Irx1, Irx2, Irx3, Irx5*, and *Irx6* in individual MN subclusters; the expression of each *Irx* gene based on scRNA-seq data is remarkably consistent with our RNA FISH/immunostaining data (Figures 2A–2O). Altogether, our analysis provides a detailed expression map of *Irx* genes in post-mitotic spinal MNs, uncovering molecular markers for subpopulations of embryonic MMC and LMC neurons (Figures 2P and 2Q).

IRX6 is expressed in human motor neurons derived from embryonic stem cells

To determine whether IRX expression in MNs is a conserved feature from mice to human, we generated MNs from a human embryonic stem cell (hESC) line (HUES3 Hb9/Mnx1GFP).[61] Following differentiation of the HUES3 line and immunofluorescence (see Materials and Methods), we found that IRX6 co-localizes with HB9/MNX1 in human post-mitotic MNs (day 21 in culture) (Figure S2). Because the differentiation protocol we used is known to generate LMC neurons,[62] IRX6 is likely expressed in human LMC neurons, consistent with the *Irx6* expression in the mouse spinal cord (Figures 2M–2O). In addition to detecting IRX6, we also tested several commercially available antibodies against human IRX2, IRX3, and IRX5, but failed to detect specific signal in hESC-derived MNs (Table S1).

Irx2, *Irx5*, and *Irx6* are expressed in LMC neurons at brachial and lumbar domains

To determine *Irx* expression in MNs along the rostrocaudal axis of the spinal cord, we examined thoracic and lumbar domains at e12.5. Similar to brachial domains, MMC neurons of thoracic and lumbar domains also express *Irx2* (Figure S3). Hence, *Irx2* marks post-mitotic MMC neurons along the embryonic spinal cord. Unlike MMC neurons, LMC neurons are only present at brachial and lumbar domains, from which they innervate forelimb and hindlimb muscles, respectively.[63] However, the extent of molecular similarity between brachial and lumbar MNs remains poorly defined as most studies focus on brachial MNs.[56] RNA ISH showed that *Irx2, Irx5,* and *Irx6* are not only expressed in subpopulations of brachial LMC neurons, but also in their lumbar counterparts (Figure S3A), a finding that we corroborated with scRNA-seq data of the lumbar e13.5 spinal cord (Figure S3B). Hence, certain *Irx* genes are expressed both in brachial and lumbar LMC neurons.

Irx2 is required for limb-innervating motor neuron development

Unlike *Irx3, Irx5,* and *Irx6*, *Irx2* is expressed in most, if not all, LMC neurons in the brachial domain of the spinal cord (Figures 2D–2F). To test whether *Irx2* is necessary for LMC neuron development, we used CRISPR/Cas9 to generate *Irx2* mutant mice, herein referred to as *Irx2* $^{\Delta 5bp/\Delta 5bp}$ because they carry a 5bp-long deletion in the 2nd exon of *Irx2* (Figure 3A) (see Materials and Methods). Consistent with previously described *Irx2* KO mice generated by classic Cre/*loxP* recombination,[64] homozygous *Irx2* $^{\Delta 5bp/\Delta 5bp}$ are viable and fertile. The 5bp deletion is predicted to cause a frameshift in the open reading frame (at codon 122), introducing a premature termination codon (Figures 3A and 3B). Such a frameshift drastically changes the amino acid composition of the Irx2 homeodomain (Figure 3B and Data S1), which is essential for DNA-binding.

In the brachial domain of *Irx2* $^{\Delta 5bp/\Delta 5bp}$ spinal cords at e12.5, we found a significant reduction in the total number of MNs, assessed by the co-expression of Hb9 and Isl1/2 (Figures 3C and 3E). Using the LMC-specific marker FoxP1, we found that this reduction specifically affects LMC neurons (Figures 3D and 3F). To identify which subpopulation of LMC neurons is affected, we stained for Pea3 (ETV4), which marks a specific subgroup of LMC neurons that innervate back muscles in mice.[59] We found no difference in the number of Pea3-expressing MNs between control (*Irx2*$^{+/+}$) and *Irx2* $^{\Delta 5bp/\Delta 5bp}$ mice (Figure 3G). We conclude that the number of LMC neurons located outside the Pea3 pool (Foxp1+ Pea3-) is reduced in the brachial spinal cord of *Irx2* mutant animals.

Axonal projections and forelimb grip strength are unaffected in *Irx2* mutants

Because *Irx* genes are involved in axon guidance in the retina,[37] we wondered whether *Irx2* is required for motor axon guidance. To visualize MN axons, we crossed the *Irx2* $^{\Delta 5bp/\Delta 5bp}$ animals to *Hb9(Mnx1)::GFP* mice and performed wholemount GFP immunostaining at e12.5. Compared to control mice, MN axonal projections to forelimb and trunk (cutaneous maximus) muscles appear grossly normal in *Irx2* $^{\Delta 5bp/\Delta 5bp}$ animals (Figures 3H and 3I). Next, we reasoned that the reduced numbers of LMC neurons in *Irx2* $^{\Delta 5bp/\Delta 5bp}$ mice may affect forelimb grip strength, as LMC neurons specifically innervate forelimb muscles. However, we did not observe a statistically significant effect in adult *Irx2* $^{\Delta 5bp/\Delta 5bp}$ animals compared to controls (Figure S4). Altogether, we observe a modest decrease in the number of brachial LMC neurons in *Irx2* $^{\Delta 5bp/\Delta 5bp}$ mice, but no significant effects on axon guidance and forelimb grip strength.

Irx5 is not required for brachial motor neuron generation and axon guidance

Like *Irx2*, *Irx5* is expressed in LMC neurons (Figures 2J and 2L). To test whether *Irx5* controls aspects of LMC development, we

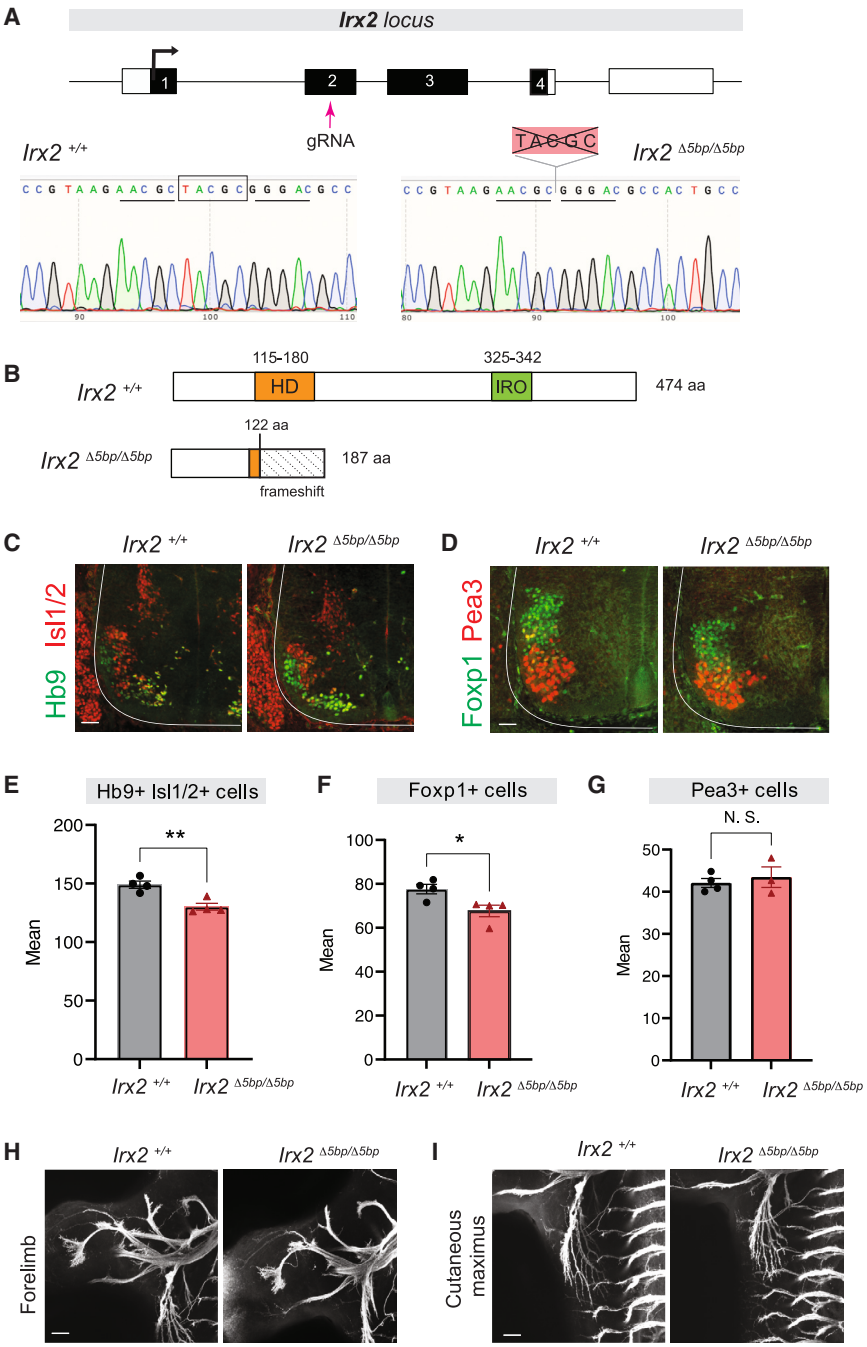

Figure 3. Generation and characterization of *Irx2* mutant mice

(A) A gRNA targets exon 2 of *Irx2*. Representative chromatograms of genotyped mice demonstrate the 5bp (TACGC) deletion in *Irx2* $^{\Delta 5bp/\Delta 5bp}$ mice.

(B) Wild-type and truncated Irx2 proteins in the *Irx2* $^{\Delta 5bp}$ mouse. See text for details.

(C and D) Double immunostaining for Hb9 (green) and Isl1/2 (red) (panel C) or Foxp1 (green) and Pea3 (red) (panel D) in e12.5 wild-type and *Irx2* $^{\Delta 5bp/\Delta 5bp}$ spinal cords. ($N = 4$). Scale bar: 50μm.

(E–G) Quantification of Hb9+/Isl1/2+, Foxp1+, or Pea3+ MNs in *Irx2* $^{\Delta 5bp/\Delta 5bp}$ mice at e12.5 ($N = 4$). $^{*}p < 0.05$, $^{**}p < 0.01$, $^{***}p < 0.001$, N. S.: Not significant. Analyses performed using unpaired *t*-test (two-tailed). Data are shown as mean ± SEM.

(H and I) MN axons labeled with Hb9::GFP in control and *Irx2* $^{\Delta 5bp/\Delta 5bp}$ mice at e12.5 ($N = 4$). Projections to forelimb (H) and cutaneous maximus (I) muscle. Scale bar: 50 μm. See also Figure S4.

employed CRISPR/Cas9 to generate *Irx5* mutant mice, which carry a 5bp-long deletion in the 1st exon of *Irx5* (Figures 4A and 4B) (see Materials and Methods). Homozygous *Irx5* $^{\Delta 5bp/\Delta 5bp}$ mice are viable. This deletion is predicted to result in a premature termination codon, likely generating a truncated protein that lacks both the HD and IRO domains (Figure 4B and Data S1). Antibody staining showed dramatically reduced Irx5 protein expression in *Irx5* $^{\Delta 5bp/\Delta 5bp}$ spinal cords at e12.5 (Figure 4C), indicating *Irx5* $^{\Delta 5bp}$ is a loss-of-function allele. However, quantification of either all brachial MNs (Hb9+ cells) (Figures 4D and 4F), only LMC neurons (Foxp1+ cells) (Figures 4E and 4G), or MNs of the Pea3 population (Pea3+ cells) (Figures 4E and 4H) did not reveal any differences between control and *Irx5* $^{\Delta 5bp/\Delta 5bp}$ animals at e12.5. Similarly, the number of brachial MNs expressing ChAT and Isl1/2 is unaltered at postnatal day 10 (p10) (Figures 4I–4K). Further, MN axonal projections to forelimb and trunk (cutaneous maximus) muscles appear grossly normal in *Irx5* $^{\Delta 5bp/\Delta 5bp}$ animals (Figures 4L and 4M). We conclude that *Irx5* is not required for brachial MN generation or axon guidance, raising the possibility that *Irx5* acts redundantly with *Irx6* given their overlapping expression in LMC neurons (Figure 2).

Irx6 limits the number of brachial MNs in the mouse spinal cord

Due to its restricted expression in a subpopulation of LMC neurons (Pea3 pool and three additional MN subclusters) (Figure 2P), we mutated *Irx6* to test whether it is required for LMC development. We used CRISPR/Cas9 to generate *Irx6* mutant mice that carry a 19bp-long deletion in the 2nd of the six *Irx6* exons (Figure 5A) (see Materials and Methods). Homozygous *Irx6* $^{\Delta 19bp/\Delta 19bp}$ mice are viable. The deletion is predicted to generate a truncated protein lacking both the HD and IRO domains (Figure 5B and Data S1). Next, we quantified the number of LMC neurons (Foxp1+ cells) at consecutive sections along the rostrocaudal axis of the e12.5 brachial spinal cord. Compared to control *Irx6* $^{+/+}$ mice, we found a significant

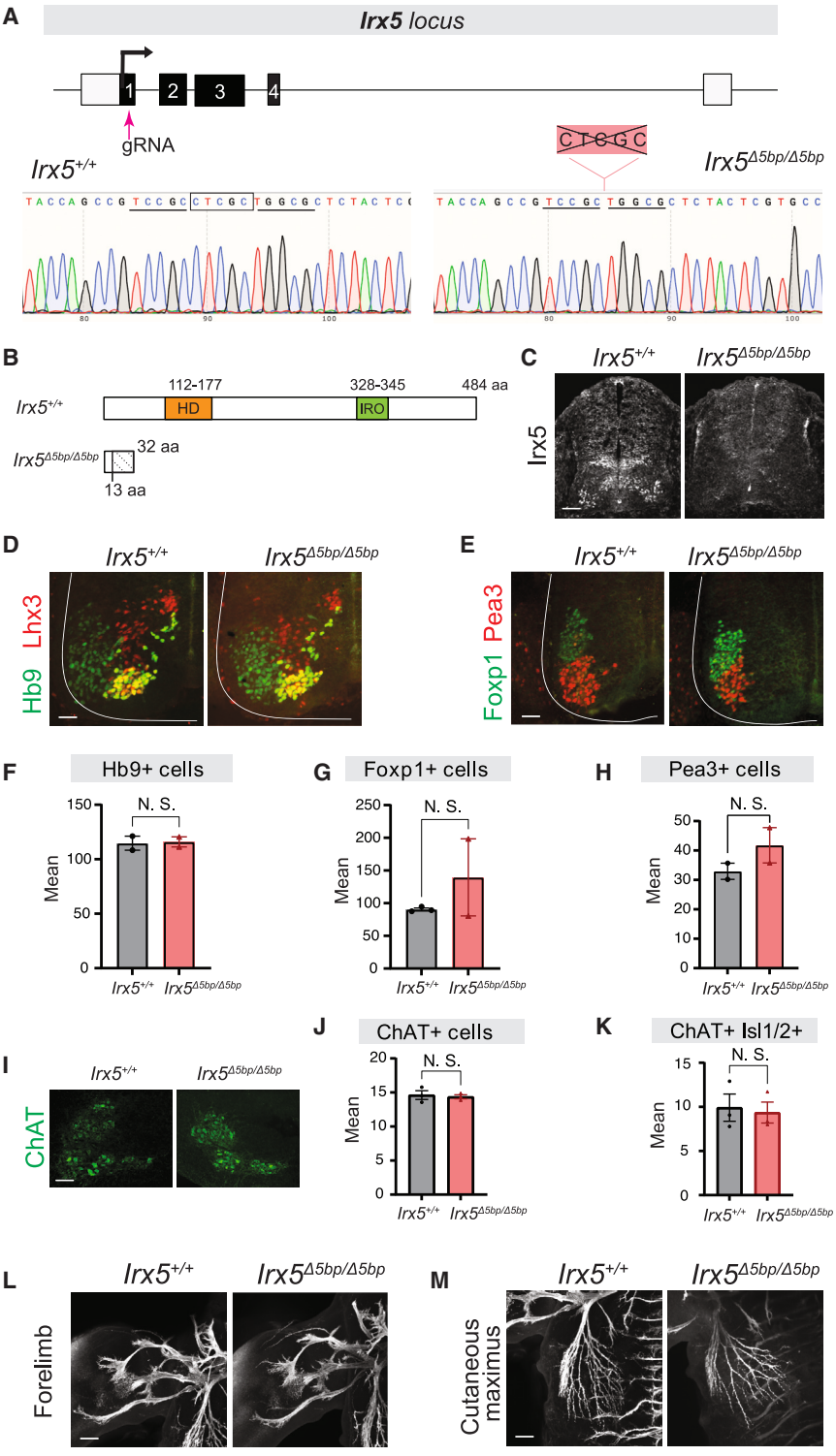

Figure 4. Generation and characterization of *Irx5* mutant mice

(A) A gRNA targets exon 1 of *Irx5*. Representative chromatograms of genotyped mice illustrate the 5 bp (CTCGC) deletion in *Irx5* $^{\Delta 5bp/\ \Delta 5bp}$.

(B) Wild-type and truncated Irx5 proteins produced in the *Irx5* $^{\Delta 5bp}$ mouse. Both HD and Iro domains are removed in the *Irx5* $^{\Delta 5bp}$ protein.

(C) Immunohistochemistry shows strong reduction in Irx5 expression in *Irx5* $^{\Delta 5bp/\ \Delta 5bp}$ spinal cords at e12.5.

(D) Double immunohistochemistry for Hb9 and Lhx3 in control and *Irx5* $^{\Delta 5bp/\Delta 5bp}$ mice at e12.5.

(E) Double immunohistochemistry for Foxp1 and Pea3 in control and *Irx5* $^{\Delta 5bp/\Delta 5bp}$ mice at e12.5.

(F–H) Quantification of Hb9+, Foxp1+, or Pea3+ MNs in *Irx5* $^{\Delta 5bp/\ \Delta 5bp}$ mice at e12.5. $^{*}p < 0.05$, $^{**}p < 0.01$, $^{***}p < 0.001$, N. S.: Not significant. C-H: N = 2–3 for *Irx5* $^{+/\ +}$, *N* = 2 for *Irx5* $^{\Delta 5bp/\ \Delta 5bp}$. Analyses performed using unpaired *t*-test (two-tailed). Data are shown as mean ± SEM.

(I) Immunostaining shows ChAT expression in control and *Irx5* $^{\Delta 5bp/\ \Delta 5bp}$ spinal cords at p10.

(J and K) Quantification of ChAT+ (J) or ChAT+ and Isl1/2+ double-positive cells (K) in control and *Irx5* $^{\Delta 5bp/\ \Delta 5bp}$ spinal cords at p10. *N* = 3 (L-M) MN axons labeled with Hb9GFP in control and *Irx5* $^{\Delta 5bp/\ \Delta 5bp}$ mice at e12.5. Projections to forelimb (L) and cutaneous maximus (M) muscle. I-J: *N* = 3 for *Irx5* $^{+/+}$, *N* = 2 for *Irx5* $^{\Delta 5bp/\ \Delta 5bp}$. Scale bar: 50 μm.

increase in the number of Foxp1+ MNs in rostral sections of the *Irx6* $^{\Delta 19bp/\Delta 19bp}$ spinal cord (Figures 5C and 5D). This increase is not a result of abnormal generation of MN progenitors, as we found no difference in the number of Olig2+ MN progenitors between control and *Irx6* $^{\Delta 19bp/\Delta 19bp}$ spinal cords at e12.5 (Figure 5E). However, we observed a decrease ($p = 0.05$) in the number of cleaved-Caspase 3 positive cells only in the rostral region of the brachial e12.5 spinal cord (Figure 5F). Because it is known that roughly half of all spinal MNs in mice are eliminated through programmed cell death between e12.5 and e15.5[65,66], it is likely that *Irx6* is required for developmental MN cell death in the rostral LMC. We conclude that *Irx6* has a relatively minor role in the developing spinal cord to limit the number of LMC neurons in brachial (rostral) domains.

Hoxc8 controls *Irx2*, *Irx5*, and *Irx6* expression in brachial motor neurons

In the developing spinal cord, expression of *Irx3* in progenitor cells is regulated by Shh signaling.[31,49] In post-mitotic neurons, however, little is known about *Irx* gene regulation. At the brachial (mostly caudal) domain of the mouse spinal cord, the transcription factor *Hoxc8* controls various facets of MN development including axon guidance and terminal differentiation.[58,67] Our

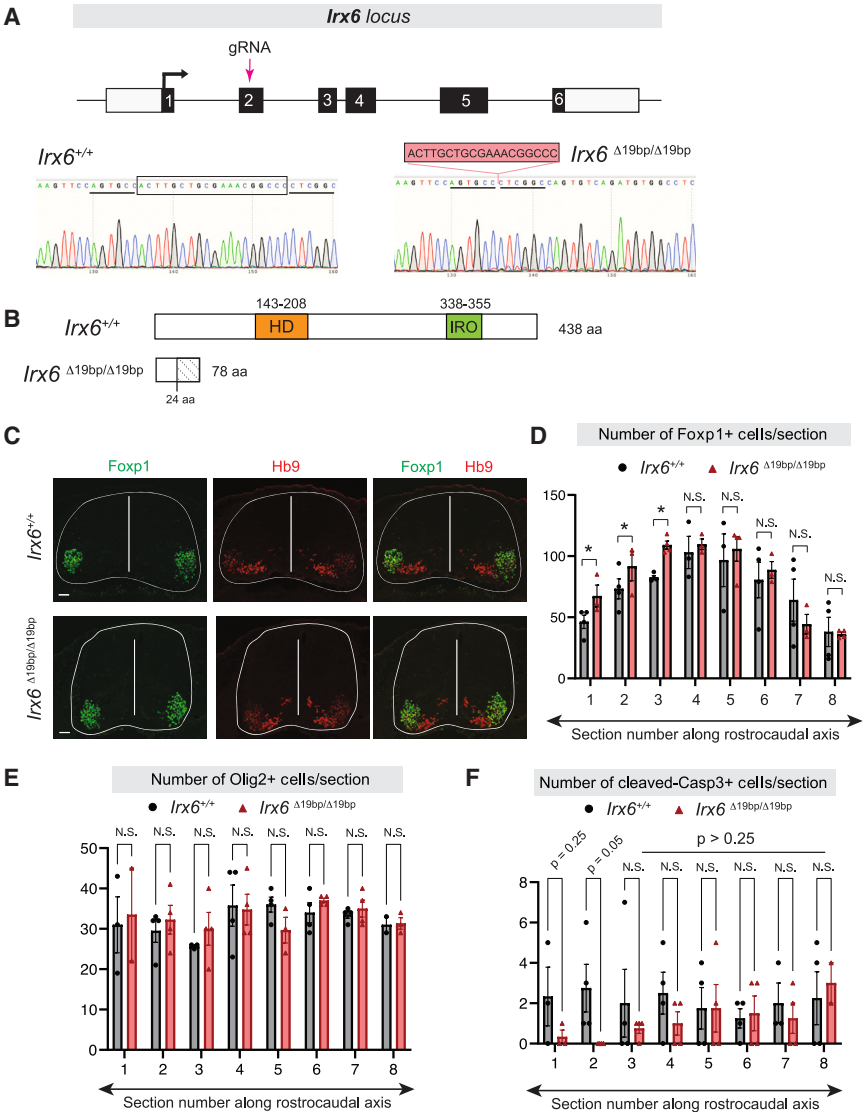

Figure 5. Generation and characterization of *Irx6* mutant mice

(A) A gRNA targets exon 2 of *Irx6* locus. Representative chromatograms of genotyped mice illustrate the 19 bp deletion in the *Irx6* $^{\Delta 19bp/\ \Delta 19bp}$ mouse.

(B) Wildtype and truncated Irx6 proteins produced in the *Irx6*$^{\Delta 19bp}$ mouse. HD and Iro domains are removed in the *Irx6* $^{\Delta 19bp}$ protein.

(C) Antibody staining for Foxp1-expressing MNs (green) and Hb9-positive MNs (red) in control (*Irx6* $^{+/+}$) and *Irx6* $^{\Delta 19bp/\Delta 19bp}$ spinal cords at e12.5. $N = 4$. Scale bar: 50 μm.

(D) Quantifications of Foxp1+ MNs along the rostro-caudal axis reveal an increased number of LMC MNs in rostral sections of the *Irx6* $^{\Delta 19bp/\Delta 19bp}$ spinal cord at e12.5 ($N = 4$). *$p < 0.05$, **$p < 0.01$, ***$p < 0.001$, N. S.: Not significant. Analyses performed using unpaired *t*-test (two-tailed). Data are shown as mean ± SEM.

(E and F) Quantification of Olig2+ progenitor cells (E) or cleaved-Caspase-3+ cells (F) along the rostro-caudal axis of control and *Irx6* $^{\Delta 19bp/\Delta 19bp}$ spinal cords at e12.5 ($N = 4$). N. S.: Not significant.

scRNA-seq data analysis revealed co-expression of *Hoxc8* and *Irx* genes in brachial caudal MNs (Figure 6A), raising the hypothesis that Hoxc8 may also control *Irx* gene expression in these MNs.

To test this, we crossed homozygous mice carrying a conditional *Hoxc8* allele (*Hoxc8* $^{fl/fl}$) to *Olig2*^{Cre} mice that enable *Cre* recombinase expression specifically in MN progenitors,[68] thus effectively removing *Hoxc8* gene activity from their descendant post-mitotic MNs before e12.5.[67] Post-mitotic MNs in mice are generated between e9 - e11.[69] Because e12.5 is an early stage of MN differentiation we will refer to the *Olig2*^{Cre}*::Hoxc8* $^{fl/fl}$ mice as *Hoxc8 MNΔ* ^{early}. In the LMC neurons of these mice at e12.5, we found through RNA ISH that expression of *Irx2* is reduced specifically in the caudal region of the *Hoxc8 MNΔ* ^{early} brachial spinal cord (Figure 6B). Further, *Irx5* and *Irx6* expression is undetectable in the brachial (caudal) spinal cord of *Hoxc8 MNΔ* ^{early} mice at e12.5 (Figure 6C). These effects are not an indirect consequence of MN cell loss as the total number of brachial MNs is unaffected in *Hoxc8 MNΔ* ^{early} animals at e12.5.[67] We conclude that Hoxc8 is required during development (at e12.5 or earlier) to activate *Irx2, Irx5* and *Irx6* expression in young post-mitotic LMC neurons.

How is *Irx* gene expression maintained in post-mitotic MNs? Because *Hoxc8* and *Irx* genes continue to be expressed in LMC neurons during developmental and postnatal stages (Figure 2),[67,70] we asked whether Hoxc8 is required to maintain *Irx* expression in LMC neurons. We crossed the *Hoxc8*$^{fl/fl}$ mice with the *Chat*^{IRESCre} mouse line, which enables efficient gene inactivation in post-mitotic MNs around e13.5 – e14.5.[67,71] We refer to the *Chat*^{IRESCre}*::Hoxc8*$^{fl/fl}$ animals as *Hoxc8 MNΔ* ^{late} because *Hoxc8* depletion in MNs occurs later compared to *Hoxc8 MNΔ* ^{early} mice. Interestingly, *Irx2* expression is unaffected in brachial (caudal) MNs of *Hoxc8 MNΔ* ^{late} mice at p8 (Figure 6B). However, expression of *Irx5* and *Irx6* is reduced at p8 (Figure 6B). Altogether, our findings on *Hoxc8 MNΔ* ^{early} and *Hoxc8 MNΔ* ^{late} mice demonstrate that, in brachial (caudal) LMC neurons, Hoxc8 is required to induce *Irx2*, *Irx5* and *Irx6* during early development, as well as to maintain *Irx5* and *Irx6* during later developmental stages.

Hoxc8 likely acts directly to control *Irx* gene expression in mouse motor neurons

To gain mechanistic insights on *Irx* gene regulation, we analyzed available chromatin immunoprecipitation sequencing (ChIP-seq) datasets on MNs derived from mouse embryonic stem cells

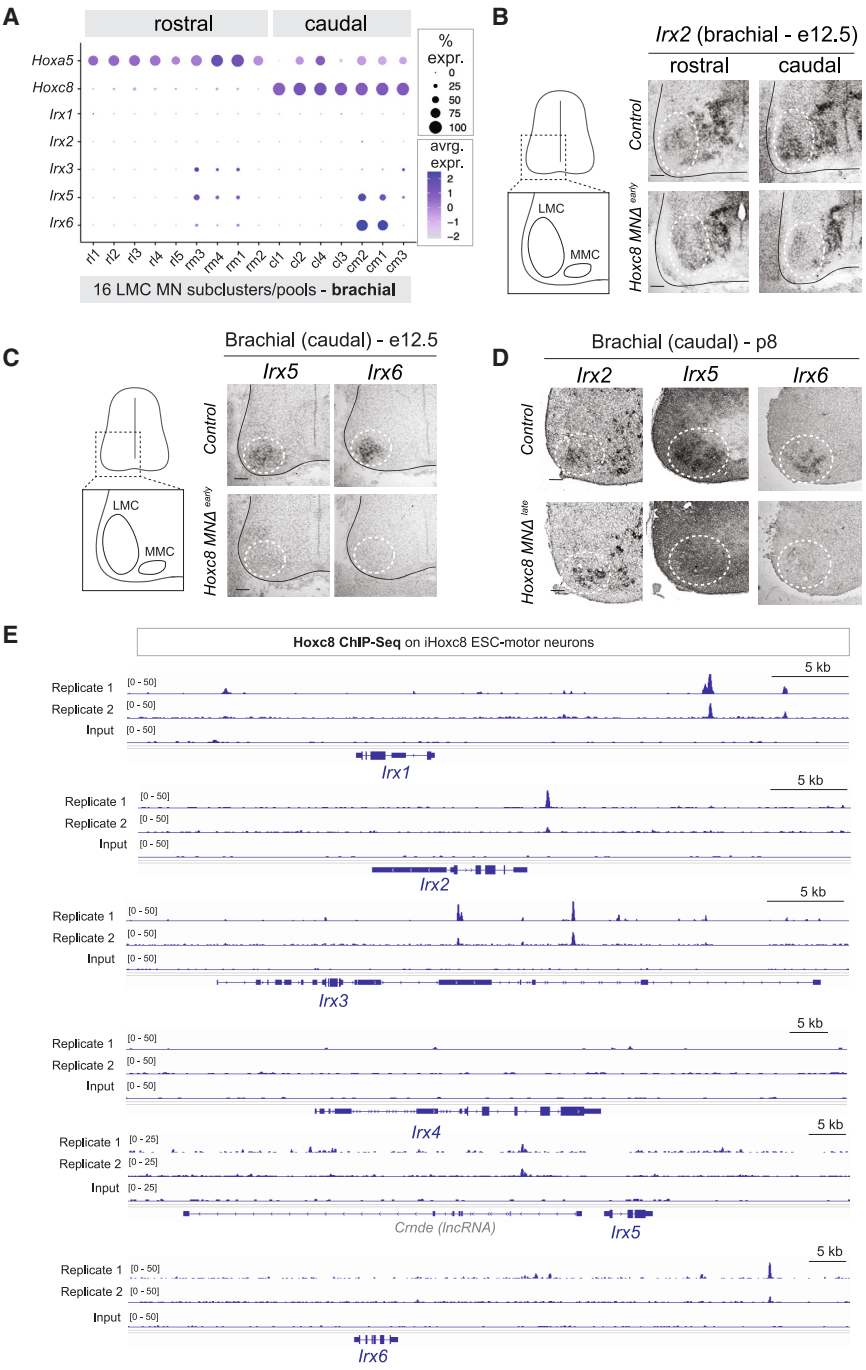

Figure 6. Hoxc8 controls *Irx* expression in spinal motor neurons

(A) Dot plot showing *Irx* expression in the brachial mouse spinal cord at e13.5. scRNA-Seq data analyzed from.[56] *Hoxc8* is selectively expressed in the caudal domain of the brachial spinal cord.

(B) RNA ISH shows reduced *Irx2* expression in the caudal (not rostral) domain of the brachial *Hoxc8 MNΔ*^{early} spinal cord at e12.5 (N = 4).

(C) *Irx5* and *Irx6* expression is reduced in e12.5 *Hoxc8 MNΔ*^{early} spinal cords (N = 4).

(D) At p8, *Irx5* and *Irx6* expression is reduced in *Hoxc8 MNΔ*^{late} spinal cords, but *Irx2* expression is unaffected (N = 4). Scale bar: 50 μm.

(E) Analysis of ChIP-Seq data from iHoxc8 MNs shows Hoxc8 directly binds to the *cis*-regulatory region of *Irx* genes. GEO accession numbers: Input (GSM4226461) and iHoxc8 replicates (GSM4226436, GSM4226437). Snapshots of each gene locus were generated with Integrative Genomics Viewer (IGV, Broad Institute).

(mESCs), in which *Hoxc8* expression was induced with doxycycline.[72] In this context, ChIP-seq for Hoxc8 revealed binding in the *cis*-regulatory region of *Irx1, Irx2, Irx3, Irx5,* and *Irx6* genes. No binding was observed *on Irx4*, the only *Irx* gene not expressed in spinal MNs (Figures 1D and 6E). The ChIP-seq data, together with our *in vivo* findings in *Hoxc8* MN*Δ* ^{early} and *Hoxc8* MN*Δ* ^{late} mice, suggest that Hoxc8 likely acts directly to activate *Irx* gene expression in spinal MNs (Figure 7E).

LIN-39/Hox directly activates *irx-1* in *C. elegans* motor neurons

Both vertebrate and invertebrate *Irx/Iro* genes are regulated by Hedgehog and TGF-b signaling pathways,[22,49,76] suggesting control mechanisms regulating *Irx/Iro* gene expression are under strong evolutionary pressure and thereby conserved across distant species. To test whether the role of Hox genes in regulating *Irx/Iro* expression is deeply conserved, we turned to the nematode *C. elegans*, which is evolutionarily separated from mice by hundreds of millions of years (Figure 1A). In the *C. elegans* ventral nerve cord (analogous to the mouse spinal cord), MNs that control locomotion co-express the Hox gene *lin-39 (Scr/Dfd/Hox3-5)* and the sole *Irx/Iro C. elegans* ortholog, *irx-1*.[77] We observed a significant reduction in the number of MNs expressing an *irx-1::gfp* reporter in *lin-39/Hox* loss-of-function (LOF) mutant animals at the fourth larval stage (L4) (Figures 7A and 7B). Because nerve cord MNs that control locomotion are normally generated in *lin-39* mutant animals,[78] we conclude that *irx-1* expression in *C. elegans* MNs requires positive LIN-39/Hox input. Further, we analyzed available LIN-39 ChIP-seq data at L3,[73] a stage by which all *irx-1*-expressing MNs have been generated. Similar to our Hoxc8 observations in mouse MNs, LIN-39 *(Scr/Dfd/Hox3-5)* binds directly to the *cis*-regulatory region of *irx-1* (Figure 7C). Altogether, our findings in *C. elegans* and mouse MNs uncover an ancient role for Hox proteins in the regulation of *Irx* gene expression (Figures 7D and 7E).

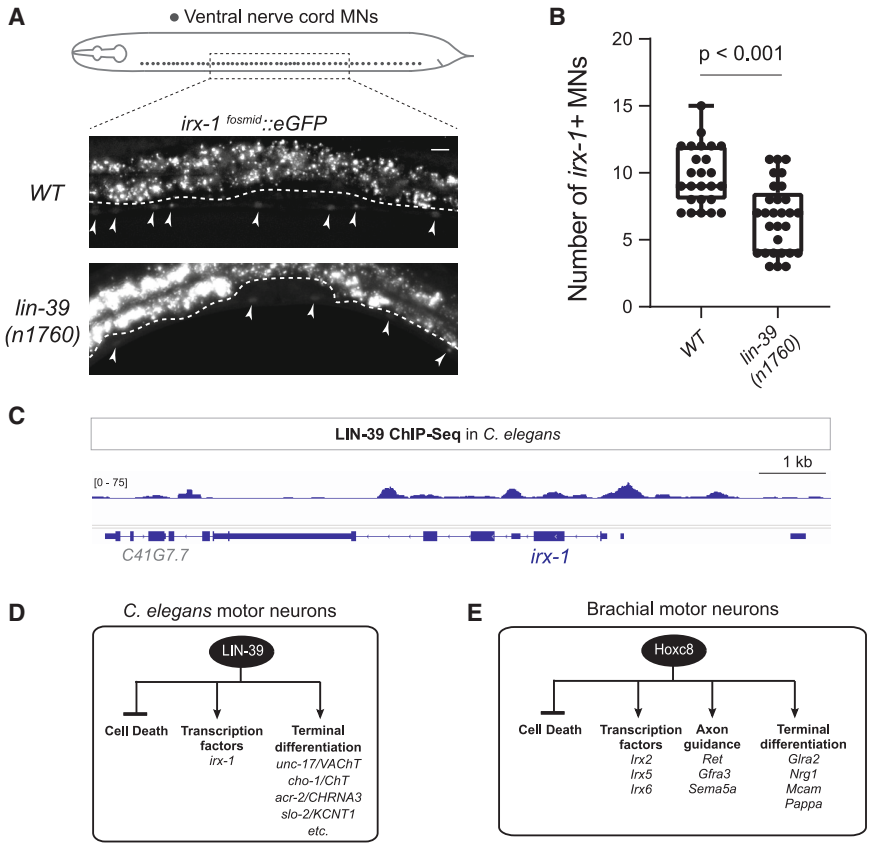

Figure 7. LIN-39/Hox controls *irx-1* expression in *C. elegans* motor neurons

(A) MN cell body position along the *C. elegans* ventral nerve cord. Expression of an *irx-1::eGFP* reporter *(wgIs536)* is decreased in MNs of *C. elegans* animals carrying the *lin-39* (*n1760*) LOF allele. A 300μm region of the ventral nerve cord (VNC) was analyzed at the fourth larval stage (L4). Anterior is left, dorsal is up. Arrowheads point to MN nuclei. Green fluorescence signal is shown in white for better contrast. Scale bar: 5 μm.

(B) Quantification of total number of MNs expressing *irx-1* in WT and *lin-39* null mutants. Box and whiskers plot show the min, max and quartiles with single data points annotated. WT: $N = 25$, *lin-39* mutant: $N = 30$.

(C) ChIP-Seq tracks are shown for LIN-39 on *irx-1*. The modENCODE project generated the ChIP-Seq data for LIN-39.[73]

(D) Schematic of known LIN-39 functions and target genes in *C. elegans* MNs. See discussion for details. A complete list of terminal differentiation genes regulated by LIN-39 in *C. elegans* MNs can be found in.[74,75]

(E) Schematic of known Hoxc8 functions and target genes in brachial MNs. See discussion for details. Target genes of Hoxc8 with roles in axon guidance and terminal differentiation have been previously described.[58,67]

DISCUSSION

The expression, function, and regulation of *Irx*/*Iro* homeobox genes in the nervous system is poorly defined. In this study, we provide a detailed expression map of all six mouse *Irx* genes in the developing spinal cord, revealing unique and overlapping sites of expression in post-mitotic MNs. Further, we uncover a requirement for mouse *Irx2* and *Irx6* in MN development. Lastly, we show – both in *C. elegans* and mouse MNs – that HOX transcription factors positively regulate *Irx* gene expression, exposing an ancient gene regulatory relationship between two highly conserved families of clustered transcription factors.

Irx genes: Another example of a homeobox gene family critical for MN development

Locomotion is an ancient behavior displayed by invertebrate and vertebrate animals. It is therefore likely that evolutionary pressure led to a considerable degree of conservation in the molecular mechanisms that control the development and function of various cell types essential for locomotion. This is particularly evident at the level of MNs. Accumulating evidence suggests that highly conserved gene regulatory programs control MN development. For example, the homeobox transcription factor HB9/Mnx1, which is transiently expressed in developing MNs, specifies MN subtype identity in worms, flies, simple chordates, and vertebrates.[79–83] Perhaps the most striking example of conserved regulators of MN development comes from Hox genes, a family of chromosomally clustered homeobox genes. During worm, fly and mouse MN development, region-specific expression of Hox proteins along the anterior-posterior axis of the nervous system is required for the early steps of MN development (e.g., cell specification, circuit assembly).[57] Here, we show that members of the *Irx* homeobox gene family are expressed in worm, mouse and human MNs, consistent with previous *C. elegans* studies and mouse transcriptomic datasets.[70,77,84] Further, *Irx* genes are expressed in MNs of the little skate, *Leucoraja erinacea*, a marine species of jawed vertebrates, sharing a common ancestor with tetrapods.[85] The remarkable conservation in *Irx* MN expression suggests critical functions. Consistent with this idea, *irx-1* controls MN connectivity in *C. elegans*,[77] and our data uncover essential roles for *Irx2* and *Irx6* in mouse spinal MN development. Altogether, our findings on *Irx* genes together with previous studies on Hox, HB9/Mnx1, and other LIM homeodomain protein-encoding genes lend support to the notion that homeobox genes from different families (e.g., IRX, HOX, LIM) play crucial roles in MN development.

Irx genes in the developing spinal cord: Essential and redundant roles

To date, our understanding of *Irx* gene function in the developing spinal cord has been limited to *Irx3*. Distinct classes of spinal neurons are generated at defined D-V positions in response to antiparallel morphogenetic gradients (e.g., Shh, BMP, and Wnt).[86] A set of homeodomain transcription factors is

known to act as intermediaries of Shh activity and fall into two classes: class I proteins are repressed by Shh, and class II proteins are activated by it. The expression of these proteins defines distinct progenitor domains in the chick, mouse and human spinal cord,[31,49,87] thereby generating distinct classes of neurons along the D-V axis of the spinal cord. Sharp boundaries between these progenitor domains are maintained via mutual cross-repression of class I and II proteins. In this context, *Irx3* is a class I protein that represses two class II proteins (Olig2, Nkx2.2).[29,31]

In this study, we describe essential but opposing roles for *Irx2* and *Irx6* genes in spinal MN development. The mouse mutant phenotypes suggest that *Irx2* promotes the generation of LMC (Foxp1+) neurons in the entire brachial domain of the spinal cord (Figure 3), whereas *Irx6* limits the generation of these neurons specifically in rostral domains of the brachial spinal cord (Figure 5). Although the underlying molecular mechanisms for these phenotypes remain elusive, the decreased numbers of cleaved-Caspase-3 positive cells in *Irx6* $^{\Delta 19bp/\Delta 19bp}$ spinal cords suggest a possible pro-apoptotic role for *Irx6* in brachial (rostral) MNs. We did not observe any phenotypes in our *Irx5* mutant animals, possibly due to genetic redundancy with *Irx6*. Of note, *Irx5* is known to act redundantly with other *Irx* genes in the context of heart development.[88] However, the neighboring position of *Irx5* and *Irx6* on the same chromosome prevented us from generating double *Irx5*$^{\Delta 5bp/\Delta 5bp}$; *Irx6*$^{\Delta 19bp/\Delta 19bp}$ mutant mice by genetic crossing (Figure 1B).

The *Irx* genes constitute ancient Hox targets in motor neurons

An interesting aspect of *Irx* genes is their conserved patterns of expression. Within vertebrate lineages, the expression of *Irx* orthologs is largely equivalent, suggesting conservation of their *cis*-regulatory elements. For example, all vertebrate *Irx3* orthologs are expressed in equivalent regions of the neural tube and lateral mesoderm.[20,53,89] Further, both vertebrate and invertebrate *Iro/Irx* genes are regulated by Hedgehog and TGF-beta signaling,[22,49,76] suggesting that *cis*-regulatory elements controlling the ancestral *Iro/Irx* gene have been evolutionarily conserved. Our findings support this idea and expand our understanding of *Iro/Irx* gene regulation in the following ways.

First, we show that *Irx* genes are regulated by Hox transcription factors both in *C. elegans* and mouse MNs, exposing an ancient gene regulatory relationship. Second, ChIP-seq data for *C. elegans* LIN-39/Hox and mouse Hoxc8 provide mechanistic insights supporting a model of direct regulation of *Irx* genes by Hox transcription factors. (Figures 6 and 7). The selective binding of Hoxc8 to *cis*-regulatory regions of *Irx* genes expressed in MNs (*Irx1*, *Irx2*, *Irx3*, *Irx5*, and *Irx6*) suggests the presence of MN-specific enhancers driving *Irx* expression. The binding regions of LIN-39/Hox and Hoxc8 onto *Irx* genes provide a starting point for future functional assays to identify such enhancers in *C. elegans* and mice. Such assays can be of biomedical relevance. For example, enhancer activity of *Irx3* and *Irx5* in the hypothalamus, a brain region involved in feeding behavior and metabolism, has been linked to obesity.[42–45] Last, while it is known that Shh represses *Irx3* along the D-V axis, how *Irx* genes are regulated along the anteroposterior axis of the spinal cord remains unknown. We found that *Irx* genes are expressed in MNs of the brachial, thoracic, and lumbar domains. Like the action of Hoxc8 in brachial MNs, other Hox proteins may regulate *Irx* gene expression in thoracic and lumbar domain MNs.

Expanding the repertoire of Hox target genes in the nervous system

HOX transcription factors play fundamental roles in hindbrain and spinal cord development.[57,90,91] Yet, their downstream target genes in the nervous system remain poorly defined. Our study expands the known repertoire of Hox target genes in the nervous system. Both in *C. elegans* and mouse MNs, we show that Hox transcription factors activate *Irx* gene expression. However, future experiments (e.g., enhancer deletion) are required to investigate whether Hox proteins act as direct activators of *Irx* gene transcription. Intriguingly, the functional roles for Hox in *C. elegans* and mouse MN development appear highly conserved. In *C. elegans*, LIN-39/Hox prevents cell death of a specific MN subtype,[92,93] but is also required more broadly for the terminal differentiation program of ventral nerve cord MNs (Figure 7D).[74,75,94] In the mouse spinal cord, global *Hoxc8* KO studies established that *Hoxc8* is needed to prevent MN cell death,[95] and conditional KO approaches showed that it promotes axon guidance and terminal differentiation of brachial MNs (Figure 7E).[58,67] Since global inactivation of either *Hoxc8* or *Irx2* results in decreased numbers of brachial MNs, we speculate that *Irx2* may act as an intermediary factor – downstream of Hoxc8 – to prevent MN cell death (Figure 7E).

Limitations of the study

We found five *Irx* genes (*Irx1*, *Irx2*, *Irx3*, *Irx5*, and *Irx6*) to be expressed in post-mitotic spinal MNs in the mouse embryo. Although we uncovered a requirement for *Irx2* and *Irx6* in MN development, conditional mutagenesis is needed to determine whether *Irx2* and *Irx6* act at the level of progenitor cells or post-mitotic MNs. Due to their overlapping expression in spinal MNs and reported *Irx* heterodimerization in cardiomyocytes (i.e., Irx3, Irx4, and Irx5 physically interact),[96] combined mutant analysis is needed to uncover possible redundant roles for *Irx* genes in the spinal cord. Lastly, we recently reported continuous *Irx* gene expression in mouse spinal MNs during early postnatal and adult life.[67,70] Hence, the *Irx* expression map we describe here is likely preserved throughout post-embryonic life. Inducible mutagenesis is therefore needed to determine the complete repertoire of *Irx* gene functions in MNs at different stages of embryonic and postnatal life.

RESOURCE AVAILABILITY

Lead contact

Further information and requests for resources and reagents should be directed to and will be fulfilled by the lead contact, Paschalis Kratsios (pkratsios@uchicago.edu).

Materials availability

This study did not generate new unique reagents.

Data and code availability

- Data: All data generated or analyzed in this study are included in the manuscript and supporting files. Microscopy data reported in this paper will be shared by the lead contact upon request.

- Code: This paper does not report original code.
- Additional information: Any additional information required to reanalyze the data reported in this paper is available from the lead contact (P.K.) upon request.

ACKNOWLEDGMENTS

We thank members of the Kratsios lab (Ian Weigle, Mira Antonopoulos, Jayson J. Smith, Nidhi Sharma, Filipe Marques, Honorine Destain, Manasa Prahlad) for comments on the manuscript and Dr. Jeremy Dasen (NYU) for providing antibodies (rabbit anti-Foxp1, rabbit anti-Lhx3, rabbit anti-Hb9, rabbit anti-Isl1/2). We thank Shirley Liau for scRNA-seq data analysis, Jayson J. Smith for help with figure design and the University of Chicago Transgenic Mouse Facility (RRID:SCR_019171) and its technical director (Linda Degenstein) for generating *Irx2*, *Irx5*, and *Irx6* mutant mice using CRISPR-Cas9 genome editing. The *C. elegans* strains were provided by the CGC, which is funded by NIH Office of Research Infrastructure Programs (P40 OD010440). This work was supported by the Lohengrin Foundation and the National Institute of Neurological Disorders and Stroke (NINDS) (Award Number: R01NS116365 to P.K.).

AUTHOR CONTRIBUTIONS

Conceptualization: C.C. and P.K.; methodology: C.C., S.A., Y.C., W.F., and K.T.; investigation: C.C., S.A., Y.C., W.F., and K.T.; formal analysis: C.C., S.A., Y.C., W.F., and K.T.; visualization: C.C. and P.K.; funding acquisition: P.K.; writing – original draft: P.K.; Writing – review and editing: C.C., S.A., Y.C., W.F., and K.T.; Supervision: P.K.

DECLARATION OF INTERESTS

The authors declare no competing interests.

STAR★METHODS

Detailed methods are provided in the online version of this paper and include the following:

- KEY RESOURCES TABLE
- EXPERIMENTAL MODEL AND STUDY PARTICIPANTS DETAILS
  - Mouse husbandry and genetics
  - Human cell line
  - *C. elegans* strain maintenance
- METHOD DETAILS
  - Mouse tissue collection, processing, and immunofluorescence
  - RNA *in situ* hybridization
  - RNA fluorescent *in situ* hybridization coupled with antibody staining
  - Forelimb grip strength test
  - Differentiation of human motor neurons from embryonic stem cells
  - Immunocytochemistry on human motor neurons
  - Imaging of *irx-1* reporter gene expression in *C. elegans* MNs
- QUANTIFICATION AND STATISTICAL ANALYSIS

SUPPLEMENTAL INFORMATION

Supplemental information can be found online at https://doi.org/10.1016/j.isci.2025.112210.

Received: July 27, 2024
Revised: January 3, 2025
Accepted: March 10, 2025
Published: March 12, 2025

REFERENCES

1. Cavodeassi, F., Modolell, J., and Gómez-Skarmeta, J.L. (2001). The Iroquois family of genes: from body building to neural patterning. Development *128*, 2847–2855.
2. Gomez-Skarmeta, J.L., and Modolell, J. (2002). Iroquois genes: genomic organization and function in vertebrate neural development. Curr. Opin. Genet. Dev. *12*, 403–408. https://doi.org/10.1016/s0959-437x(02)00317-9.
3. Leyns, L., Gómez-Skarmeta, J.L., and Dambly-Chaudière, C. (1996). iroquois: a prepattern gene that controls the formation of bristles on the thorax of Drosophila. Mech. Dev. *59*, 63–72. https://doi.org/10.1016/0925-4773(96)00577-1.
4. Burglin, T.R. (1997). Analysis of TALE superclass homeobox genes (MEIS, PBC, KNOX, Iroquois, TGIF) reveals a novel domain conserved between plants and animals. Nucleic Acids Res. *25*, 4173–4180. https://doi.org/10.1093/nar/25.21.4173.
5. Peters, T., Dildrop, R., Ausmeier, K., and Rüther, U. (2000). Organization of mouse Iroquois homeobox genes in two clusters suggests a conserved regulation and function in vertebrate development. Genome Res. *10*, 1453–1462. https://doi.org/10.1101/gr.144100.
6. Gomez-Skarmeta, J.L., and Modolell, J. (1996). araucan and caupolican provide a link between compartment subdivisions and patterning of sensory organs and veins in the Drosophila wing. Genes Dev. *10*, 2935–2945. https://doi.org/10.1101/gad.10.22.2935.
7. McNeill, H., Yang, C.H., Brodsky, M., Ungos, J., and Simon, M.A. (1997). mirror encodes a novel PBX-class homeoprotein that functions in the definition of the dorsal-ventral border in the Drosophila eye. Genes Dev. *11*, 1073–1082. https://doi.org/10.1101/gad.11.8.1073.
8. Kim, K.H., Rosen, A., Bruneau, B.G., Hui, C.C., and Backx, P.H. (2012). Iroquois homeodomain transcription factors in heart development and function. Circ. Res. *110*, 1513–1524. https://doi.org/10.1161/CIRCRESAHA.112.265041.
9. van Tuyl, M., Liu, J., Groenman, F., Ridsdale, R., Han, R.N.N., Venkatesh, V., Tibboel, D., and Post, M. (2006). Iroquois genes influence proximodistal morphogenesis during rat lung development. Am. J. Physiol. Lung Cell. Mol. Physiol. *290*, L777–L789. https://doi.org/10.1152/ajplung.00293.2005.
10. Alarcon, P., Rodriguez-Seguel, E., Fernandez-Gonzalez, A., Rubio, R., and Gomez-Skarmeta, J.L. (2008). A dual requirement for Iroquois genes during Xenopus kidney development. Development *135*, 3197–3207. https://doi.org/10.1242/dev.023697.
11. Reggiani, L., Raciti, D., Airik, R., Kispert, A., and Brändli, A.W. (2007). The prepattern transcription factor Irx3 directs nephron segment identity. Genes Dev. *21*, 2358–2370. https://doi.org/10.1101/gad.450707.
12. Ragvin, A., Moro, E., Fredman, D., Navratilova, P., Drivenes, Ø., Engström, P.G., Alonso, M.E., de la Calle Mustienes, E., Gómez Skarmeta, J.L., Tavares, M.J., et al. (2010). Long-range gene regulation links genomic type 2 diabetes and obesity risk regions to HHEX, SOX4, and IRX3. Proc. Natl. Acad. Sci. USA *107*, 775–780. https://doi.org/10.1073/pnas.0911591107.
13. Jorgensen, J.S., and Gao, L. (2005). Irx3 is differentially up-regulated in female gonads during sex determination. Gene Expr. Patterns *5*, 756–762. https://doi.org/10.1016/j.modgep.2005.04.011.
14. McDonald, L.A., Gerrelli, D., Fok, Y., Hurst, L.D., and Tickle, C. (2010). Comparison of Iroquois gene expression in limbs/fins of vertebrate embryos. J. Anat. *216*, 683–691. https://doi.org/10.1111/j.1469-7580.2010.01233.x.
15. Bonnard, C., Strobl, A.C., Shboul, M., Lee, H., Merriman, B., Nelson, S.F., Ababneh, O.H., Uz, E., Güran, T., Kayserili, H., et al. (2012). Mutations in IRX5 impair craniofacial development and germ cell migration via SDF1. Nat. Genet. *44*, 709–713. https://doi.org/10.1038/ng.2259.
16. Holmquist Mengelbier, L., Lindell-Munther, S., Yasui, H., Jansson, C., Esfandyari, J., Karlsson, J., Lau, K., Hui, C.C., Bexell, D., Hopyan, S., and Gisselsson, D. (2019). The Iroquois homeobox proteins IRX3 and IRX5 have distinct roles in Wilms tumour development and human nephrogenesis. J. Pathol. *247*, 86–98. https://doi.org/10.1002/path.5171.

17. Somerville, T.D.D., Simeoni, F., Chadwick, J.A., Williams, E.L., Spencer, G.J., Boros, K., Wirth, C., Tholouli, E., Byers, R.J., and Somervaille, T.C.P. (2018). Derepression of the Iroquois Homeodomain Transcription Factor Gene IRX3 Confers Differentiation Block in Acute Leukemia. Cell Rep. *22*, 638–652. https://doi.org/10.1016/j.celrep.2017.12.063.

18. Al Sayed, Z.R., Canac, R., Cimarosti, B., Bonnard, C., Gourraud, J.B., Hamamy, H., Kayserili, H., Girardeau, A., Jouni, M., Jacob, N., et al. (2021). Human model of IRX5 mutations reveals key role for this transcription factor in ventricular conduction. Cardiovasc. Res. *117*, 2092–2107. https://doi.org/10.1093/cvr/cvaa259.

19. Kim, K.H., and Backx, P.H. (2021). Understanding the role of Iroquois homeobox transcription factor 5 (IRX5) in cardiac function: getting to the (human) heart of the matter. Cardiovasc. Res. *117*, 1989–1991. https://doi.org/10.1093/cvr/cvab098.

20. Bellefroid, E.J., Kobbe, A., Gruss, P., Pieler, T., Gurdon, J.B., and Papalopulu, N. (1998). Xiro3 encodes a Xenopus homolog of the Drosophila Iroquois genes and functions in neural specification. EMBO J. *17*, 191–203. https://doi.org/10.1093/emboj/17.1.191.

21. Glavic, A., Silva, F., Aybar, M.J., Bastidas, F., and Mayor, R. (2004). Interplay between Notch signaling and the homeoprotein Xiro1 is required for neural crest induction in Xenopus embryos. Development *131*, 347–359. https://doi.org/10.1242/dev.00945.

22. Gomez-Skarmeta, J., de La Calle-Mustienes, E., and Modolell, J. (2001). The Wnt-activated Xiro1 gene encodes a repressor that is essential for neural development and downregulates Bmp4. Development *128*, 551–560. https://doi.org/10.1242/dev.128.4.551.

23. Gomez-Skarmeta, J.L., Diez del Corral, R., de la Calle-Mustienes, E., Ferré-Marcó, D., and Modolell, J. (1996). Araucan and caupolican, two members of the novel iroquois complex, encode homeoproteins that control proneural and vein-forming genes. Cell *85*, 95–105. https://doi.org/10.1016/s0092-8674(00)81085-5.

24. Gomez-Skarmeta, J.L., Glavic, A., de la Calle-Mustienes, E., Modolell, J., and Mayor, R.X. (1998). a Xenopus homolog of the Drosophila Iroquois complex genes, controls development at the neural plate. EMBO J. *17*, 181–190. https://doi.org/10.1093/emboj/17.1.181.

25. Glavic, A., Gómez-Skarmeta, J.L., and Mayor, R. (2002). The homeoprotein Xiro1 is required for midbrain-hindbrain boundary formation. Development *129*, 1609–1621. https://doi.org/10.1242/dev.129.7.1609.

26. Itoh, M., Kudoh, T., Dedekian, M., Kim, C.H., and Chitnis, A.B. (2002). A role for iro1 and iro7 in the establishment of an anteroposterior compartment of the ectoderm adjacent to the midbrain-hindbrain boundary. Development *129*, 2317–2327. https://doi.org/10.1242/dev.129.10.2317.

27. Lecaudey, V., Anselme, I., Rosa, F., and Schneider-Maunoury, S. (2004). The zebrafish Iroquois gene iro7 positions the r4/r5 boundary and controls neurogenesis in the rostral hindbrain. Development *131*, 3121–3131. https://doi.org/10.1242/dev.01190.

28. Kobayashi, D., Kobayashi, M., Matsumoto, K., Ogura, T., Nakafuku, M., and Shimamura, K. (2002). Early subdivisions in the neural plate define distinct competence for inductive signals. Development *129*, 83–93. https://doi.org/10.1242/dev.129.1.83.

29. Mizuguchi, R., Sugimori, M., Takebayashi, H., Kosako, H., Nagao, M., Yoshida, S., Nabeshima, Y., Shimamura, K., and Nakafuku, M. (2001). Combinatorial roles of olig2 and neurogenin2 in the coordinated induction of pan-neuronal and subtype-specific properties of motoneurons. Neuron *31*, 757–771.

30. Parker, H.J., Bronner, M.E., and Krumlauf, R. (2016). The vertebrate Hox gene regulatory network for hindbrain segmentation: Evolution and diversification: Coupling of a Hox gene regulatory network to hindbrain segmentation is an ancient trait originating at the base of vertebrates. Bioessays *38*, 526–538. https://doi.org/10.1002/bies.201600010.

31. Sagner, A., and Briscoe, J. (2019). Establishing neuronal diversity in the spinal cord: a time and a place. Development *146*, dev182154. https://doi.org/10.1242/dev.182154.

32. Cheng, C.W., Yan, C.H.M., Hui, C.C., Strähle, U., and Cheng, S.H. (2006). The homeobox gene irx1a is required for the propagation of the neurogenic waves in the zebrafish retina. Mech. Dev. *123*, 252–263. https://doi.org/10.1016/j.mod.2005.12.001.

33. Choy, S.W., Cheng, C.W., Lee, S.T., Li, V.W.T., Hui, M.N.Y., Hui, C.C., Liu, D., and Cheng, S.H. (2010). A cascade of irx1a and irx2a controls shh expression during retinogenesis. Dev. Dyn. *239*, 3204–3214. https://doi.org/10.1002/dvdy.22462.

34. Mazzoni, E.O., Celik, A., Wernet, M.F., Vasiliauskas, D., Johnston, R.J., Cook, T.A., Pichaud, F., and Desplan, C. (2008). Iroquois complex genes induce co-expression of rhodopsins in Drosophila. PLoS Biol. *6*, e97. https://doi.org/10.1371/journal.pbio.0060097.

35. Pichaud, F., and Casares, F. (2000). homothorax and iroquois-C genes are required for the establishment of territories within the developing eye disc. Mech. Dev. *96*, 15–25. https://doi.org/10.1016/s0925-4773(00)00372-5.

36. Cheng, C.W., Chow, R.L., Lebel, M., Sakuma, R., Cheung, H.O.L., Thanabalasingham, V., Zhang, X., Bruneau, B.G., Birch, D.G., Hui, C.c., et al. (2005). The Iroquois homeobox gene, Irx5, is required for retinal cone bipolar cell development. Dev. Biol. *287*, 48–60. https://doi.org/10.1016/j.ydbio.2005.08.029.

37. Jin, Z., Zhang, J., Klar, A., Chédotal, A., Rao, Y., Cepko, C.L., and Bao, Z.Z. (2003). Irx4-mediated regulation of Slit1 expression contributes to the definition of early axonal paths inside the retina. Development *130*, 1037–1048. https://doi.org/10.1242/dev.00326.

38. Star, E.N., Zhu, M., Shi, Z., Liu, H., Pashmforoush, M., Sauve, Y., Bruneau, B.G., and Chow, R.L. (2012). Regulation of retinal interneuron subtype identity by the Iroquois homeobox gene Irx6. Development *139*, 4644–4655. https://doi.org/10.1242/dev.081729.

39. Matsumoto, K., Nishihara, S., Kamimura, M., Shiraishi, T., Otoguro, T., Uehara, M., Maeda, Y., Ogura, K., Lumsden, A., and Ogura, T. (2004). The prepattern transcription factor Irx2, a target of the FGF8/MAP kinase cascade, is involved in cerebellum formation. Nat. Neurosci. *7*, 605–612. https://doi.org/10.1038/nn1249.

40. Cheng, C.W., Yan, C.H.M., Choy, S.W., Hui, M.N.Y., Hui, C.C., and Cheng, S.H. (2007). Zebrafish homologue irx1a is required for the differentiation of serotonergic neurons. Dev. Dyn. *236*, 2661–2667. https://doi.org/10.1002/dvdy.21272.

41. Dou, Z., Son, J.E., and Hui, C.C. (2021). Irx3 and Irx5 - Novel Regulatory Factors of Postnatal Hypothalamic Neurogenesis. Front. Neurosci. *15*, 763856. https://doi.org/10.3389/fnins.2021.763856.

42. de Araujo, T.M., and Velloso, L.A. (2020). Hypothalamic IRX3: A New Player in the Development of Obesity. Trends Endocrinol. Metabol. *31*, 368–377. https://doi.org/10.1016/j.tem.2020.01.002.

43. Sobreira, D.R., Joslin, A.C., Zhang, Q., Williamson, I., Hansen, G.T., Farris, K.M., Sakabe, N.J., Sinnott-Armstrong, N., Bozek, G., Jensen-Cody, S.O., et al. (2021). Extensive pleiotropism and allelic heterogeneity mediate metabolic effects of IRX3 and IRX5. Science *372*, 1085–1091. https://doi.org/10.1126/science.abf1008.

44. Son, J.E., Dou, Z., Kim, K.H., Wanggou, S., Cha, V.S.B., Mo, R., Zhang, X., Chen, X., Ketela, T., Li, X., et al. (2021). Irx3 and Irx5 in Ins2-Cre(+) cells regulate hypothalamic postnatal neurogenesis and leptin response. Nat. Metab. *3*, 701–713. https://doi.org/10.1038/s42255-021-00382-y.

45. Son, J.E., Dou, Z., Wanggou, S., Chan, J., Mo, R., Li, X., Huang, X., Kim, K.H., Michaud, J.L., and Hui, C.C. (2021). Ectopic expression of Irx3 and Irx5 in the paraventricular nucleus of the hypothalamus contributes to defects in Sim1 haploinsufficiency. Sci. Adv. *7*, eabh4503. https://doi.org/10.1126/sciadv.abh4503.

46. Cavodeassi, F., Diez Del Corral, R., Campuzano, S., and Domínguez, M. (1999). Compartments and organising boundaries in the Drosophila eye: the role of the homeodomain Iroquois proteins. Development *126*, 4933–4942. https://doi.org/10.1242/dev.126.22.4933.

47. Zeidler, M.P., Perrimon, N., and Strutt, D.I. (1999). Polarity determination in the Drosophila eye: a novel role for unpaired and JAK/STAT signaling. Genes Dev. *13*, 1342–1353. https://doi.org/10.1101/gad.13.10.1342.

48. Janssens, S., Denayer, T., Deroo, T., Van Roy, F., and Vleminckx, K. (2010). Direct control of Hoxd1 and Irx3 expression by Wnt/beta-catenin signaling during anteroposterior patterning of the neural axis in Xenopus. Int. J. Dev. Biol. *54*, 1435–1442. https://doi.org/10.1387/ijdb.092985sj.

49. Briscoe, J., Pierani, A., Jessell, T.M., and Ericson, J. (2000). A homeodomain protein code specifies progenitor cell identity and neuronal fate in the ventral neural tube. Cell *101*, 435–445.

50. Houweling, A.C., Dildrop, R., Peters, T., Mummenhoff, J., Moorman, A.F., Rüther, U., and Christoffels, V.M. (2001). Gene and cluster-specific expression of the Iroquois family members during mouse development. Mech. Dev. *107*, 169–174. https://doi.org/10.1016/s0925-4773(01)00451-8.

51. Mummenhoff, J., Houweling, A.C., Peters, T., Christoffels, V.M., and Rüther, U. (2001). Expression of Irx6 during mouse morphogenesis. Mech. Dev. *103*, 193–195. https://doi.org/10.1016/s0925-4773(01)00353-7.

52. Bosse, A., Stoykova, A., Nieselt-Struwe, K., Chowdhury, K., Copeland, N.G., Jenkins, N.A., and Gruss, P. (2000). Identification of a novel mouse Iroquois homeobox gene, Irx5, and chromosomal localisation of all members of the mouse Iroquois gene family. Dev. Dyn. *218*, 160–174. https://doi.org/10.1002/(SICI)1097-0177(200005)218:1<160::AID-DVDY14>3.0.CO;2-2.

53. Bosse, A., Zülch, A., Becker, M.B., Torres, M., Gómez-Skarmeta, J.L., Modolell, J., and Gruss, P. (1997). Identification of the vertebrate Iroquois homeobox gene family with overlapping expression during early development of the nervous system. Mech. Dev. *69*, 169–181. https://doi.org/10.1016/s0925-4773(97)00165-2.

54. Cohen, D.R., Cheng, C.W., Cheng, S.H., and Hui, C.C. (2000). Expression of two novel mouse Iroquois homeobox genes during neurogenesis. Mech. Dev. *91*, 317–321. https://doi.org/10.1016/s0925-4773(99)00263-4.

55. Christoffels, V.M., Keijser, A.G., Houweling, A.C., Clout, D.E., and Moorman, A.F. (2000). Patterning the embryonic heart: identification of five mouse Iroquois homeobox genes in the developing heart. Dev. Biol. *224*, 263–274. https://doi.org/10.1006/dbio.2000.9801.

56. Liau, E.S., Jin, S., Chen, Y.C., Liu, W.S., Calon, M., Nedelec, S., Nie, Q., and Chen, J.A. (2023). Single-cell transcriptomic analysis reveals diversity within mammalian spinal motor neurons. Nat. Commun. *14*, 46. https://doi.org/10.1038/s41467-022-35574-x.

57. Philippidou, P., and Dasen, J.S. (2013). Hox genes: choreographers in neural development, architects of circuit organization. Neuron *80*, 12–34. https://doi.org/10.1016/j.neuron.2013.09.020.

58. Catela, C., Shin, M.M., Lee, D.H., Liu, J.P., and Dasen, J.S. (2016). Hox Proteins Coordinate Motor Neuron Differentiation and Connectivity Programs through Ret/Gfralpha Genes. Cell Rep. *14*, 1901–1915. https://doi.org/10.1016/j.celrep.2016.01.067.

59. Livet, J., Sigrist, M., Stroebel, S., De Paola, V., Price, S.R., Henderson, C.E., Jessell, T.M., and Arber, S. (2002). ETS gene Pea3 controls the central position and terminal arborization of specific motor neuron pools. Neuron *35*, 877–892.

60. Martinez, T.L., Kong, L., Wang, X., Osborne, M.A., Crowder, M.E., Van Meerbeke, J.P., Xu, X., Davis, C., Wooley, J., Goldhamer, D.J., et al. (2012). Survival motor neuron protein in motor neurons determines synaptic integrity in spinal muscular atrophy. J. Neurosci. *32*, 8703–8715. https://doi.org/10.1523/JNEUROSCI.0204-12.2012.

61. Di Giorgio, F.P., Boulting, G.L., Bobrowicz, S., and Eggan, K.C. (2008). Human embryonic stem cell-derived motor neurons are sensitive to the toxic effect of glial cells carrying an ALS-causing mutation. Cell Stem Cell *3*, 637–648. https://doi.org/10.1016/j.stem.2008.09.017.

62. Amoroso, M.W., Croft, G.F., Williams, D.J., O'Keeffe, S., Carrasco, M.A., Davis, A.R., Roybon, L., Oakley, D.H., Maniatis, T., Henderson, C.E., and Wichterle, H. (2013). Accelerated high-yield generation of limb-innervating motor neurons from human stem cells. J. Neurosci. *33*, 574–586. https://doi.org/10.1523/JNEUROSCI.0906-12.2013.

63. Dalla Torre di Sanguinetto, S.A., Dasen, J.S., and Arber, S. (2008). Transcriptional mechanisms controlling motor neuron diversity and connectivity. Curr. Opin. Neurobiol. *18*, 36–43. https://doi.org/10.1016/j.conb.2008.04.002.

64. Lebel, M., Agarwal, P., Cheng, C.W., Kabir, M.G., Chan, T.Y., Thanabalasingham, V., Zhang, X., Cohen, D.R., Husain, M., Cheng, S.H., et al. (2003). The Iroquois homeobox gene Irx2 is not essential for normal development of the heart and midbrain-hindbrain boundary in mice. Mol. Cell Biol. *23*, 8216–8225. https://doi.org/10.1128/MCB.23.22.8216-8225.2003.

65. Lance-Jones, C. (1982). Motoneuron cell death in the developing lumbar spinal cord of the mouse. Brain Res. *256*, 473–479. https://doi.org/10.1016/0165-3806(82)90192-4.

66. Oppenheim, R.W., Houenou, L.J., Johnson, J.E., Lin, L.F., Li, L., Lo, A.C., Newsome, A.L., Prevette, D.M., and Wang, S. (1995). Developing motor neurons rescued from programmed and axotomy-induced cell death by GDNF. Nature *373*, 344–346. https://doi.org/10.1038/373344a0.

67. Catela, C., Chen, Y., Weng, Y., Wen, K., and Kratsios, P. (2022). Control of spinal motor neuron terminal differentiation through sustained Hoxc8 gene activity. Elife *11*, e70766. https://doi.org/10.7554/eLife.70766.

68. Zawadzka, M., Rivers, L.E., Fancy, S.P.J., Zhao, C., Tripathi, R., Jamen, F., Young, K., Goncharevich, A., Pohl, H., Rizzi, M., et al. (2010). CNS-resident glial progenitor/stem cells produce Schwann cells as well as oligodendrocytes during repair of CNS demyelination. Cell Stem Cell *6*, 578–590. https://doi.org/10.1016/j.stem.2010.04.002.

69. Sims, T.J., and Vaughn, J.E. (1979). The generation of neurons involved in an early reflex pathway of embryonic mouse spinal cord. J. Comp. Neurol. *183*, 707–719. https://doi.org/10.1002/cne.901830403.

70. Smith, J.J., Taylor, S.R., Blum, J.A., Feng, W., Collings, R., Gitler, A.D., Miller, D.M., 3rd, and Kratsios, P. (2024). A molecular atlas of adult C. elegans motor neurons reveals ancient diversity delineated by conserved transcription factor codes. Cell Rep. *43*, 113857. https://doi.org/10.1016/j.celrep.2024.113857.

71. Philippidou, P., Walsh, C.M., Aubin, J., Jeannotte, L., and Dasen, J.S. (2012). Sustained Hox5 gene activity is required for respiratory motor neuron development. Nat. Neurosci. *15*, 1636–1644. https://doi.org/10.1038/nn.3242.

72. Bulajic, M., Srivastava, D., Dasen, J.S., Wichterle, H., Mahony, S., and Mazzoni, E.O. (2020). Differential abilities to engage inaccessible chromatin diversify vertebrate Hox binding patterns. Development *147*, dev194761. https://doi.org/10.1242/dev.194761.

73. Boyle, A.P., Araya, C.L., Brdlik, C., Cayting, P., Cheng, C., Cheng, Y., Gardner, K., Hillier, L.W., Janette, J., Jiang, L., et al. (2014). Comparative analysis of regulatory information and circuits across distant species. Nature *512*, 453–456. https://doi.org/10.1038/nature13668.

74. Feng, W., Destain, H., Smith, J.J., and Kratsios, P. (2022). Maintenance of neurotransmitter identity by Hox proteins through a homeostatic mechanism. Nat. Commun. *13*, 6097. https://doi.org/10.1038/s41467-022-33781-0.

75. Feng, W., Li, Y., Dao, P., Aburas, J., Islam, P., Elbaz, B., Kolarzyk, A., Brown, A.E., and Kratsios, P. (2020). A terminal selector prevents a Hox transcriptional switch to safeguard motor neuron identity throughout life. Elife *9*, e50065. https://doi.org/10.7554/eLife.50065.

76. Cavodeassi, F., Rodríguez, I., and Modolell, J. (2002). Dpp signalling is a key effector of the wing-body wall subdivision of the Drosophila mesothorax. Development *129*, 3815–3823. https://doi.org/10.1242/dev.129.16.3815.

77. Petersen, S.C., Watson, J.D., Richmond, J.E., Sarov, M., Walthall, W.W., and Miller, D.M., 3rd. (2011). A transcriptional program promotes remodeling of GABAergic synapses in Caenorhabditis elegans. J. Neurosci. *31*, 15362–15375. https://doi.org/10.1523/JNEUROSCI.3181-11.2011.

78. Stefanakis, N., Carrera, I., and Hobert, O. (2015). Regulatory Logic of Pan-Neuronal Gene Expression in C. elegans. Neuron *87*, 733–750. https://doi.org/10.1016/j.neuron.2015.07.031.

79. Arber, S., Han, B., Mendelsohn, M., Smith, M., Jessell, T.M., and Sockanathan, S. (1999). Requirement for the homeobox gene Hb9 in the consolidation of motor neuron identity. Neuron *23*, 659–674. https://doi.org/10.1016/s0896-6273(01)80026-x.

80. Broihier, H.T., and Skeath, J.B. (2002). Drosophila homeodomain protein dHb9 directs neuronal fate via crossrepressive and cell-nonautonomous mechanisms. Neuron *35*, 39–50. https://doi.org/10.1016/s0896-6273(02)00743-2.

81. Hudson, C., Ba, M., Rouvière, C., and Yasuo, H. (2011). Divergent mechanisms specify chordate motoneurons: evidence from ascidians. Development *138*, 1643–1652. https://doi.org/10.1242/dev.055426.

82. Von Stetina, S.E., Fox, R.M., Watkins, K.L., Starich, T.A., Shaw, J.E., and Miller, D.M., 3rd. (2007). UNC-4 represses CEH-12/HB9 to specify synaptic inputs to VA motor neurons in C. elegans. Genes Dev. *21*, 332–346. https://doi.org/10.1101/gad.1502107.

83. Thaler, J., Harrison, K., Sharma, K., Lettieri, K., Kehrl, J., and Pfaff, S.L. (1999). Active suppression of interneuron programs within developing motor neurons revealed by analysis of homeodomain factor HB9. Neuron *23*, 675–687. https://doi.org/10.1016/s0896-6273(01)80027-1.

84. Delile, J., Rayon, T., Melchionda, M., Edwards, A., Briscoe, J., and Sagner, A. (2019). Single cell transcriptomics reveals spatial and temporal dynamics of gene expression in the developing mouse spinal cord. Development *146*, dev173807. https://doi.org/10.1242/dev.173807.

85. Yoo, D., Park, J., Lee, C., Song, I., Lee, Y.H., Yun, T., Lee, H., Heguy, A., Han, J.Y., Dasen, J.S., et al. (2022). Little skate genome provides insights into genetic programs essential for limb-based locomotion. Elife *11*, e78345. https://doi.org/10.7554/eLife.78345.

86. Briscoe, J., and Small, S. (2015). Morphogen rules: design principles of gradient-mediated embryo patterning. Development *142*, 3996–4009. https://doi.org/10.1242/dev.129452.

87. Rayon, T., Maizels, R.J., Barrington, C., and Briscoe, J. (2021). Single-cell transcriptome profiling of the human developing spinal cord reveals a conserved genetic programme with human-specific features. Development *148*, dev199711. https://doi.org/10.1242/dev.199711.

88. Gaborit, N., Sakuma, R., Wylie, J.N., Kim, K.H., Zhang, S.S., Hui, C.C., and Bruneau, B.G. (2012). Cooperative and antagonistic roles for Irx3 and Irx5 in cardiac morphogenesis and postnatal physiology. Development *139*, 4007–4019. https://doi.org/10.1242/dev.081703.

89. Tan, J.T., Korzh, V., and Gong, Z. (1999). Expression of a zebrafish iroquois homeobox gene, Ziro3, in the midline axial structures and central nervous system. Mech. Dev. *87*, 165–168. https://doi.org/10.1016/s0925-4773(99)00121-5.

90. Krumlauf, R. (2016). Hox Genes and the Hindbrain: A Study in Segments. Curr. Top. Dev. Biol. *116*, 581–596. https://doi.org/10.1016/bs.ctdb.2015.12.011.

91. Parker, H.J., and Krumlauf, R. (2017). Segmental arithmetic: summing up the Hox gene regulatory network for hindbrain development in chordates. Wiley Interdiscip. Rev. Dev. Biol. *6*, 1–28. https://doi.org/10.1002/wdev.286.

92. Liu, H., Strauss, T.J., Potts, M.B., and Cameron, S. (2006). Direct regulation of egl-1 and of programmed cell death by the Hox protein MAB-5 and by CEH-20, a C. elegans homolog of Pbx1. Development *133*, 641–650. https://doi.org/10.1242/dev.02234.

93. Potts, M.B., Wang, D.P., and Cameron, S. (2009). Trithorax, Hox, and TALE-class homeodomain proteins ensure cell survival through repression of the BH3-only gene egl-1. Dev. Biol. *329*, 374–385. https://doi.org/10.1016/j.ydbio.2009.02.022.

94. Kratsios, P., Kerk, S.Y., Catela, C., Liang, J., Vidal, B., Bayer, E.A., Feng, W., De La Cruz, E.D., Croci, L., Consalez, G.G., et al. (2017). An intersectional gene regulatory strategy defines subclass diversity of C. elegans motor neurons. Elife *6*, e25751. https://doi.org/10.7554/eLife.25751.

95. Tiret, L., Le Mouellic, H., Maury, M., and Brûlet, P. (1998). Increased apoptosis of motoneurons and altered somatotopic maps in the brachial spinal cord of Hoxc-8-deficient mice. Development *125*, 279–291.

96. He, W., Jia, Y., and Takimoto, K. (2009). Interaction between transcription factors Iroquois proteins 4 and 5 controls cardiac potassium channel Kv4.2 gene transcription. Cardiovasc. Res. *81*, 64–71. https://doi.org/10.1093/cvr/cvn259.

97. Brenner, S. (1974). The genetics of Caenorhabditis elegans. Genetics *77*, 71–94.

98. Dasen, J.S., Tice, B.C., Brenner-Morton, S., and Jessell, T.M. (2005). A Hox regulatory network establishes motor neuron pool identity and target-muscle connectivity. Cell *123*, 477–491. https://doi.org/10.1016/j.cell.2005.09.009.

99. De Marco Garcia, N.V., and Jessell, T.M. (2008). Early motor neuron pool identity and muscle nerve trajectory defined by postmitotic restrictions in Nkx6.1 activity. Neuron *57*, 217–231. https://doi.org/10.1016/j.neuron.2007.11.033.

100. Schindelin, J., Arganda-Carreras, I., Frise, E., Kaynig, V., Longair, M., Pietzsch, T., Preibisch, S., Rueden, C., Saalfeld, S., Schmid, B., et al. (2012). Fiji: an open-source platform for biological-image analysis. Nat. Methods *9*, 676–682. https://doi.org/10.1038/nmeth.2019.

101. Takeshita, H., Yamamoto, K., Nozato, S., Inagaki, T., Tsuchimochi, H., Shirai, M., Yamamoto, R., Imaizumi, Y., Hongyo, K., Yokoyama, S., et al. (2017). Modified forelimb grip strength test detects aging-associated physiological decline in skeletal muscle function in male mice. Sci. Rep. *7*, 42323. https://doi.org/10.1038/srep42323.

102. Tsioras, K., Smith, K.C., Edassery, S.L., Garjani, M., Li, Y., Williams, C., McKenna, E.D., Guo, W., Wilen, A.P., Hark, T.J., et al. (2023). Analysis of proteome-wide degradation dynamics in ALS SOD1 iPSC-derived patient neurons reveals disrupted VCP homeostasis. Cell Rep. *42*, 113160. https://doi.org/10.1016/j.celrep.2023.113160.

STAR★METHODS

KEY RESOURCES TABLE

REAGENT or RESOURCE	SOURCE	IDENTIFIER
Antibodies		
Goat polyclonal anti-ChAT	Millipore Sigma	Cat#AB144P; RRID: AB_2079751
Rabbit monoclonal anti-Cleaved Caspase-3	Cell Signaling Technology	Cat#9664S; RRID: AB_2070042
Guinea Pig anti-Foxp1	Dasen Lab	N/A
Rabbit polyclonal anti-Foxp1	Dasen lab	CU1025; RRID: AB_2631297
Rabbit anti-Islet1/2	Jessell Lab	N/A
Rabbit Anti-Hb9	Dasen Lab	N/A
Rabbit monoclonal anti-Irx3	Abcam	Cat#ab242133; RRID: AB_3677593
Rabbit monoclonal anti-Irx5	Abcam	Cat#ab246494; RRID: AB_3677592
Rabbit polyclonal anti-Irx6	Proteintech	Cat#24440-1-AP; RRID:AB_2918082
Rabbit anti-Lhx3	Jessell Lab	N/A
Mouse monoclonal anti-Lim3/Lhx3	Developmental Studies Hybridoma Bank	Cat#67.4E12; RRID: AB_2135805
Mouse monoclonal anti-MNR2/HB9/Mnx1	Developmental Studies Hybridoma Bank	Cat#81.5C10; RRID: AB_2145209
Mouse monoclonal anti-Nkx6.1	Developmental Studies Hybridoma Bank	Cat#F55A10; RRID: AB_532378
Rabbit polyclonal anti-Olig2	Millipore Sigma	Cat#AB9610; RRID: AB_570666
Rabbit polyclonal anti-mPea3	Dasen lab	N/A
Sheep polyclonal anti-Digoxigenin-POD, Fab fragments	Roche Diagnostics Deutschland GmbH	Cat#11207733910; RRID: AB_514500
Donkey polyclonal Alexa Fluor 488 AffiniPure Anti-Guinea Pig IgG	Jackson ImmunoResearch Labs	Cat#706-545-148; RRID:AB_2340472
Donkey polyclonal Cy3 AffiniPure anti-Guinea Pig IgG	Jackson ImmunoResearch Labs	Cat#706-165-148; RRID:AB_2340460
Donkey polyclonal Alexa Fluor 488 anti-Rabbit IgG	Thermo Fisher Scientific	Cat#A-21206; RRID:AB_2535792
Donkey polyclonal Cy3 AffiniPure anti- Rabbit IgG	Jackson ImmunoResearch Labs	Cat#711-165-152; RRID:AB_2307443
Donkey polyclonal Alexa Fluor 647 anti-Rabbit IgG	Jackson ImmunoResearch Labs	Cat#711-605-152; RRID: AB_2492288
Donkey polyclonal Alexa Fluor 488 anti-mouse IgG	Thermo Fisher Scientific	Cat#A-21202; RRID:AB_141607
Donkey polyclonal Cy3 AffiniPure anti-Mouse IgG	Jackson ImmunoResearch Labs	Cat#715-165-150; RRID:AB_2340813
Goat polyclonal Alexa Fluor 488 AffiniPure anti-mouse IgG_1	Jackson ImmunoResearch Labs	Cat#115-545-205; RRID:AB_2338854
Goat polyclonal Cy3 AffiniPure anti-mouse IgG_1	Jackson ImmunoResearch Labs	Cat#115-165-205; RRID:AB_2338694
Bacterial and virus strains		
E.coli OP50	Brenner et al.[97]	N/A
Chemicals, peptides, and recombinant proteins		
mTeSR	Stem Cell Technologies	Cat#5820
N-2 Supplement (100X)	Thermo Fisher Scientific	Cat#17502001
B-27 Supplement (50X), serum free	Thermo Fisher Scientific	Cat# 17504001
GlutaMAX Supplement	Thermo Fisher Scientific	Cat#35050061
MEM Non-Essential Amino Acids Solution (100X)	Thermo Fisher Scientific	Cat# 11140050
DMEM/F-12	Thermo Fisher Scientific	Ca# 11320082
Neurobasal Medium	Thermo Fisher Scientific	Cat# 21103049
EdU	Thermo Fisher Scientific	Cat# A10044

(*Continued on next page*)

Continued

REAGENT or RESOURCE	SOURCE	IDENTIFIER
TrypLE™ Express Enzyme (1X), no phenol red	Thermo Fisher Scientific	Cat# 12604013
1X PBS	Corning	Cat# MT21040CV
Accutase	Innovative Cell Technologies	Cat# AT 104-500
SB431542	DNSK International	Cat# DNSK-KI-12
SAG	DNSK International	Cat# DNSK-SMO-1
SU5402	DNSK International	Cat# DNSK-KI-11
Y27632. 2HCl	DNSK International	Cat#DNSK-KI-15-02
Retinoic Acid	Millipore-Sigma	Cat# R2625-50MG
L-Ascorbic Acid	Millipore-Sigma	Cat#A4403-100MG
DMSO (Tissue Culture)	Millipore-Sigma	Cat# D2650-100ML
LDN 193189 dihydrochloride	Bio-Techne	Cat# 6053/10
DAPT	Bio-Techne	Cat# 2634/10
Recombinant Human BDNF Protein, CF	Bio-Techne	Cat#248-BDB-050/CF
Recombinant Human CNTF Protein, CF	Bio-Techne	Cat# 257-NT-050/CF
Recombinant Human GDNF Protein, CF	Bio-Techne	Cat# 212-GD-050/CF
Acetic anhydride	Thermo Fisher Scientific	Cat#A10-1
BCIP (5-Bromo-4-chloro-3-indolyl-phosphate)	Roche Diagnostics Deutschland GmbH	Cat# 11383221001
Blocking reagent	Roche Diagnostics Deutschland GmbH	Cat#1096176
Bovine Serum Albumin (BSA)	Thermo Fisher Scientific	Cat#BP9703-100
Coverglass (24 × 60mm, No 1)	Electron Microscopy Sciences	Cat#63770-01
50x Denhardt's Solution	Thermo Fisher Scientific	Cat# 750018
DreamTaq Green PCR Master Mix (2X)	Thermo Fisher Scientific	Cat# K1082
Formamide	Thermo Fisher Scientific	Cat#BP227-500
Hydrochloric acid	Thermo Fisher Scientific	Cat#A144-500
30% Hydrogen Peroxide	Thermo Fisher Scientific	Cat#H325-500
NBT (4-Nitro Blue Tetrazolium Chloride)	Roche Diagnostics Deutschland GmbH	Cat#11383213001
Paraformaldehyde	Millipore-Sigma	Cat#441244-1KG
Phosphate Buffered Saline (PBS) tablets	Millipore-Sigma	Cat#P4417-100TAB
ProLong Diamond Antifade Mountant with DAPI	Thermo Fisher Scientific	Cat#P36971
Salmon Sperm DNA solution	Thermo Fisher Scientific	Cat#15632011
20X SSC	Thermo Fisher Scientific	Cat#15557-036
Sucrose	Thermo Fisher Scientific	Cat#BP220-1
Tissue Plus O.C.T. Compound	Fisher Healthcare	Cat#4585
Triethanolamine	Thermo Fisher Scientific	Cat#T350-500
Triton X-100	Thermo Fisher Scientific	Cat#BP151-500
Yeast RNA	Thermo Fisher Scientific	Cat#AM7118
Critical commercial assays		
TSA Plus Cyanine3/Fluorescein System	PerkinElmer	Cat#NEL753001KT
Experimental models: Cell lines		
Human: HUES3 HB9:GFP hESC line	Di Giorgio et al.[61]	Cellosaurus ID:CVCL_X724
Experimental models: Organisms/strains		
Mouse: *Irx2* $^{\Delta 5bp/\Delta 5bp}$	This study	N/A
Mouse: *Irx5* $^{\Delta 5bp/\Delta 5bp}$	This study	N/A
Mouse: *Irx6* $^{\Delta 19bp/\Delta 19bp}$	This study	N/A
C. elegans: *lin-39(n1760)*/dpy-17(e164) unc-32(e189) *III;*	Caenorhabditis Genetics Center (CGC)	Strain:MT4009

(*Continued on next page*)

Continued

REAGENT or RESOURCE	SOURCE	IDENTIFIER
C. elegans: *unc-119(tm4063) III; wgIs536 [irx-1::TY1::EGFP::3xFLAG + unc-119 (+)]*	Caenorhabditis Genetics Center (CGC)	Strain:OP536
Oligonucleotides		
gRNA *Irx2*: GTACCGTAAGAACGCTACGC	This study	N/A
gRNA *Irx5*: GTACCAGCCGTCCGCCTCGC	This study	N/A
gRNA *Irx6*: CTTGCTGCGAAACGGCCCCT	This study	N/A
Primer: Irx2 Forward: ACAGGCTGTTGTGGGTTCC	This study	N/A
Primer: Irx2 Reverse: CATCCTGTGCCTTGTCTGAA	This study	N/A
Primer: Irx5 Forward: AGAAGCCAGGTGCCCTCTC	This study	N/A
Primer: Irx5 Reverse: CAGCTCACACTCACCACGTAA	This study	N/A
Primer: Irx6 Forward: GAGATTCTGCACCTGGTGGT	This study	N/A
Primer: Irx6 Reverse: CTTGTCCCCAGACAAGGTCACAG	This study	N/A
Recombinant DNA		
RNA ISH probes	This study; Data S2	N/A
Software and algorithms		
Fiji	ImageJ	RRID: SCR_003070; https://imagej.net/software/fiji/
Adobe Illustrator 28.7.1	Adobe Creative Cloud	N/A
Adobe Photoshop 25.12.0	Adobe Creative Cloud	N/A
Prism 9.5.1 (733)	GraphPad Software	https://www.graphpad.com/
ZEN	ZEISS	RRID: SCR_013672; https://portal.zeiss.com/download-center/softwares/mic
Other		
University of Chicago Transgenic Mouse Facility	This study	RRID:SCR_019171

EXPERIMENTAL MODEL AND STUDY PARTICIPANTS DETAILS

Mouse husbandry and genetics

All mouse procedures were approved by the Institutional Animal Care and Use Committee (IACUC) of the University of Chicago (Protocol # 72463). Morning (9a.m.) of the day on which a vaginal plug was seen was termed embryonic day 0.5 (E0.5).

The *Irx2* mutant mice were generated at the Transgenics/ES Cell Technology Mouse Core Facility of the University of Chicago. A gRNA targeting exon 2 of *Irx2* (gRNA: GTACCGTAAGAACGCTACGC) was injected into mouse zygotes together with a Cas9-expressing plasmid. Founder animals were genotyped by sequencing and a 5 bp deletion was detected in exon 2 of the *Irx2* locus (*Irx2* $^{\Delta 5bp/\Delta 5bp}$). In the F1 generation, heterozygous *Irx2* $^{\Delta 5bp/\Delta 5bp}$ mice were used for crosses to establish a homozygous mutant line. Primers for genotyping the *Irx2* $^{\Delta 5bp/\Delta 5bp}$ allele: Forward primer 5′-ACAGGCTGTTGTGGGTTCC-3′, Reverse primer 5′-CATCCT GTGCCTTGTCTGAA-3’. Using similar CRISPR/Cas9 procedures, we generated the *Irx5* $^{\Delta 5bp/\Delta 5bp}$ and *Irx6* $^{\Delta 19bp/\Delta 19bp}$ mice.

gRNA targeting *Irx5:* 5′-GTACCAGCCGTCCGCCTCGC-3’
Primers for genotyping the *Irx5* $^{\Delta 5bp/\Delta 5bp}$ allele:
Irx5 Forward 5′-AGAAGCCAGGTGCCCTCTC-3’
Irx5 Reverse 5′-CAGCTCACACTCACCACGTAA-3’
gRNA targeting Irx6: 5′-CTTGCTGCGAAACGGCCCCT-3’
Primers for genotyping the *Irx6*$^{\Delta 19bp/\Delta 19bp}$ allele:
Irx6 Forward 5′-GAGATTCTGCACCTGGTGGT-3’
Irx6 Reverse 5′-CTTGTCCCCAGACAAGGTCACAG-3’

Homozygous mice for the *Irx2* $^{\Delta 5bp/\Delta 5bp}$ allele, *Irx5* $^{\Delta 5bp/\Delta 5bp}$ allele, or *Irx6*$^{\Delta 19bp/\Delta 19bp}$ allele were analyzed at embryonic day 12.5 (e12.5), postnatal day 8 (p8), or in adult stages (6.5 and 7.6 months of age). Both sexes were included in the analysis.

Human cell line

The HUES 3 Hb9GFP (RRID:CVCL_X724) cell line used in this study has been provided by the Harvard University under a Material Transfer Agreement (MTA No: A54931). The specific cell line has been generated and characterized by Di Giorgio et al.[61] The parental line HUES 3 (RRID:CVCL_B161) is derived from the blastocyst stage and the sex of the cell is male. The HUES 3 Hb9GFP cell line was

authenticated using fluorescent microscopy as differentiated motor neurons express Hb9GFP. The HUES 3 Hb9GFP cells have been tested negative for mycoplasma using the MycoAlert PLUS detection kit by Lonza (LT07-703).

C. elegans strain maintenance

Worms were grown at 20°C on nematode growth media (NGM) plates seeded with bacteria (*E.coli* OP50) as food source.[97] Animals carrying the *lin-39 (n1760)* mutant allele were crossed with animals carrying the *wgIs536 [irx-1::TY1::EGFP::3xFLAG + unc-119 (+)]* fosmid-based reporter for *irx-1.* Hermaphrodite animals were analyzed at the fourth larval stage (L4).

METHOD DETAILS

Mouse tissue collection, processing, and immunofluorescence

Mouse embryos were harvested at E12.5 and fixed for 1.5 h in 4% paraformaldehyde in PBS at 4°C. Embryos were then washed in ice-cold PBS, equilibrated overnight in 30% sucrose/PBS at 4°C, embedded in optimal cutting temperature (OCT) compound, and sectioned at 12um on a Leica CM3050 S cryostat. For immunofluorescence staining, sections were briefly washed in PBS, blocked for 30 min in 1% BSA in PBT (PBS with 0.1% Triton X-100) at room temperature, then incubated overnight in primary antibodies (diluted in 0.1% BSA/PBT) at 4°C. Sections were then washed in PBT, incubated in secondary antibodies in PBT for 1 h at room temperature, and washed again in PBST before applying the Prolong Diamond antifade mounting medium (Invitrogen Cat #: P36971) and a coverslip. Primary and secondary antibodies are listed in key resources table.

RNA *in situ* hybridization

E12.5 embryos and p8 spinal cords were fixed in 4% paraformaldehyde for 1.5–2 h and overnight, respectively, placed in 30% sucrose/PBS overnight (4°C), and embedded in OCT compound. Cryosections were generated and processed for *in situ* hybridization or immunohistochemistry as previously described.[98,99]

RNA fluorescent *in situ* hybridization coupled with antibody staining

Cryosections were postfixed in 4% paraformaldehyde and washed in PBS. Endogenous peroxidase was blocked with a 1% H_2O_2 solution and cryosections were permeabilized in PBS/0.1% Triton X-100. Next, sections were hybridized with a DIG-labeled RNA probe overnight at 72°C, and washed in SSC. Then, the anti-DIG antibody conjugated with peroxidase (Roche) and primary antibody against Foxp1 (rabbit anti-Foxp1, Dr. Jeremy Dasen), Irx3 (rabbit anti-Irx3, Abcam), or Lhx3 (mouse anti-Lim3, Developmental Studies Hybridoma Bank) were applied overnight (4°C) to the sections. The next day, the sections were incubated with the secondary antibody (Alexa 488 donkey anti-rabbit IgG, Life Technologies, or Alexa 488 goat anti-mouse IgG_1, Jackson ImmunoResearch Labs) and detection of RNA was performed using a Cy3 Tyramide Amplification system (PerkinElmer). Images were obtained with a high-power fluorescent microscope (Zeiss Imager V2) and analyzed with Fiji software.[100]

For double RNA fluorescence *in situ* hybridization, two different probes were used, one labeled with digoxigenin and the other with biotin. Anti-DIG-peroxidase conjugated (Roche) and anti-biotin-peroxidase conjugated antibodies were used (Vector Labs). RNA was detected using a fluorescein and a Cy3 Tyramide Amplification system (PerkinElmer).

Forelimb grip strength test

The forelimb strength of male and female mice was measured using a grip strength meter from Bioseb (model BIO-GS3).[101] Control and *Irx2* $^{\Delta 5bp/\Delta 5bp}$ mice were tested at the age of 6.6–7.5 months, following the manufacturer's protocol. In brief, the meter was positioned horizontally on a heavy metal shelf (provided by the manufacturer), assembled with a grip grid. Mice were held by the tail and lowered toward the apparatus. The mice were allowed to grasp the metal grid only with their forelimbs and were then pulled backwards in the horizontal plane. The maximum force of grip was measured, and the average of six measurements (taken with a 1-min interval) were used for the analysis. Force was measured in Newtons and grams. The experimenter was blind to the genotypes.

Differentiation of human motor neurons from embryonic stem cells

For the directed differentiation of embryonic stem cells (HUES3 HB9GFP line) to post-mitotic spinal MNs, we followed a small molecule-based protocol as previously described.[102] To induce the neuralization in the culture, we used the TGF-β inhibitor SB43154 (10μM) and the Bone Morphogenetic Pathway (BMP) inhibitor LDN-193189 (100nM). In parallel, to achieve the appropriate patterning, we included in the medium retinoic acid (RA, 1uM) and the Smoothened-Agonist (SAG, 1uM) to promote caudalization and ventralization, respectively. At the second stage of the protocol (days 6–14) where MN terminal differentiation takes place, we replaced the SB43154 and LDN-193189 molecules with the (indirect) inhibitor of the Notch pathway DAPT (5uM) and the FGFR1 inhibitor SU5402 (4uM) in order to force neuronal progenitors to exit the cell cycle. After day 14, the post-mitotic MNs were replated in the presence of neurotrophic factors (BDNF, GDNF, CNTF; 10 ng/ml all) for their final maturation.

Immunocytochemistry on human motor neurons

Motor neurons derived from the HUES3 HB9GFP line were plated on day 14 on top of 1.5mm glass coverslips (Neuvitro, Fisher scientific) coated with PDL (0.1 mg/ml, 37°C overnight) and Laminin (15μg/ml, 37°C for 3h) at a density of 80,000cells/coverslip. Cells

were washed once with PBS and fixed with 4% PFA in PBS for 20 min at RT. Following fixation, cells were washed three times with PBS and permeabilized with PBS-Triton X-100 0.2% for 45 min at RT. To block the non-specific binding of primary antibody to unrelated epitopes, cells were treated with 10% normal donkey serum (Jackson ImmunoResearch) in PBS-Triton X-100 0.1%, for 1h at RT and then incubated with primary antibody, diluted in 2% Normal Donkey Serum in PBS-TritonX-100 0.1%, overnight at 4°C. The next day, coverslips were washed three times with PBS and incubated with the fluorophore-conjugated secondary antibody (Alexa Fluor 488, or Alexa Fluor 647, all from Invitrogen or Jackson ImmunoResearch) at a dilution 1:1,000 in 2% Normal Donkey Serum in PBS-Triton X-100 0.1%, for 2h at RT protected from light. Cells were washed once with PBS, incubated with DAPI 1:1,000 in PBS for 10 min at RT, then washed again three times with PBS. Coverslips were mounted on glass slides (Fisher Scientific) using Fluoromount-G (Southern Biotech).

Imaging of *irx-1* reporter gene expression in *C. elegans* MNs

Homozygous animals for the *lin-39 (n1760)* allele and the *wgIs536* reporter were anesthetized at the fourth larval stage (L4) using 100mM of sodium azide (NaN_3) and mounted on a 4% agarose pad on glass slides. Images were taken using an automated fluorescence microscope (Zeiss, Axio Imager Z2). Several z stack images (each ~1 μm thick) were acquired with Zeiss Axiocam 503 mono using the ZEN software (Version 2.3.69.1000, Blue edition). Representative images are shown following max-projection of 1–8 μm Z-stacks using the maximum intensity projection type. Image reconstruction was performed using Fiji.[100]

QUANTIFICATION AND STATISTICAL ANALYSIS

For data quantification, graphs show values expressed as mean ± standard error of the mean (SEM). All statistical analyses were performed using unpaired *t*-test (two-tailed) (GraphPad Prism software). Differences with $p < 0.05$ were considered significant. N equals number of animals analyzed. Statistical details are also included in the figure legends.